PHYSICAL REVIEW B VOLUME 14, NUMBER 2 15 JULY 1976

Nonlocal pseudopotential calculations for the electronic structure of eleven diamond and zinc-blende semiconductors*

James R. Chelikowsky†‡ and Marvin L. Cohen

Department of Physics, University of California, and Materials and Molecular Research Division, Lawrence Berkeley Laboratory, Berkeley, California 94720

(Received 23 February 1976)

An empirical nonlocal pseudopotential scheme is employed to calculate the electronic structure of eleven semiconductors: Si, Ge, α-Sn, GaP, GaAs, GaSb, InP, InAs, InSb, ZnSe, and CdTe. Band structures, reflectivity spectra, electronic densities of states, and valence charge densities are presented and compared to experimental results. Improved optical gaps, optical critical-point topologies, valence-band widths, and valence charge distributions are obtained as compared to previous local pseudopotential results.

I. INTRODUCTION

While the empirical-pseudopotential method (EPM) has been extensively applied to the diamond and zinc-blende semiconductors, studies on these materials have been based, until recently, on a simplified "local" approximation.[1] In this approach, reflectivity experiments have played a prominent role in determining the theoretical parameters that enter EPM calculations. The local approximation has proven sufficient to explain most of the optical data available for semiconductor compounds. However, if we extend the early calculations, which have invoked the local pseudopotential approximation to the valence bands and compare the results to experiment, discrepancies arise.[2-4] Specifically, high-resolution photoemission results, i.e., x-ray photoemission spectroscopy[2,5] (XPS) and ultraviolet photoemission spectroscopy[3,6] (UPS) have demonstrated that local EPM calculations obtain incorrect valence band widths, in the majority of cases, as compared with experiment.

In addition to the discrepancies which exist for the valence-band widths, local EPM calculations have produced optical response functions in discord with recent optical-modulation techniques.[7,8] Specifically, band topologies and optical critical-point symmetries as calculated by a local pseudopotential for Ge and GaAs have been found to be in error.[8] Also a consistent assignment of structure in the reflectivity spectra using local potentials has yet to be achieved.

Recent experimental advances using x rays have permitted an assessment of the pseudopotential charge densities.[9,10] While the experimental data for Si indicated that the local pseudopotential yielded a correct bonding-charge maximum, the bond shape was found to be incorrect.[9] Also recent x-ray data on InSb indicated the local pseudopotential approach overestimates the ionicity of the crystal, i.e., it yields a greater charge transfer from In to Sb than indicated by experiment.[10]

Owing to the nature of these discrepancies, it was speculated that a purely local pseudopotential technique could not yield satisfactory results, and an energy dependent and nonlocal pseudopotential should be considered.[11,12] The evidence for this reasoning was reinforced particularly by the valence-band-width discrepancy, because other one-electron approaches (which corresponded to energy-dependent nonlocal pseudopotentials) tended to yield more accurate valence bands than the local EPM approach.[5]

As a consequence of the increased amount of experimental information (e.g., XPS and UPS data) and the aforementioned failings of the local EPM, it was felt that refined nonlocal pseudopotential calculations be performed to supplement and extend the earlier local EPM calculations.[14] Therefore, an attempt to recalculate the band structures of a number of diamond and zinc-blende semiconductors has been undertaken. Using an empirical nonlocal pseudopotential scheme we have calculated the electronic properties of Si, Ge, GaAs, ZnSe, α-Sn, InSb, CdTe, GaP, GaSb, InP, and InAs.

In Sec. II the calculation techniques are outlined; in Sec. III the results of our calculations, the band structure, reflectivity spectrum, electronic density of states, and pseudo-charge-density for each compound, are presented; and in Sec. IV, some conclusions are given.

II. CALCULATION TECHNIQUES

A. Nonlocal pseudopotentials

The fundamental concept involved in a pseudopotential calculation is that the ion core can be omitted. Computationally this is crucial for it means that the deep core potential has been removed and a simple plane wave basis will yield

rapid convergence.

Simply stated, we rewrite the one-electron Hamiltonian as

$$H = p^2/2m + V_p(\vec{r}), \tag{1}$$

where

$$V_p(\vec{r}) = V(\vec{r}) + \sum_t (E_{\vec{k}} - E_t)|\, b_t\rangle\langle\, b_t\,|\,. \tag{2}$$

$V(\vec{r})$ is the true crystal potential and $|\, b_t\rangle$ is a core state with eigenvalue E_t.[11] This new potential has the same eigenvalues $E_{\vec{k}}$, but because the real potential has been cancelled in the core region by the second term in (2),[11] the resulting eigenfunctions of (1) are smoothly varying in the core region in contrast to the true eigenfunctions. While this permits the pseudoeigenfunctions to be expressed in terms of plane waves, the pseudopotential in (2) is dependent not only on the energy eigenvalues E_k, but on the l angular-momentum components present in the core states.

In spite of the fact that (2) is inherently nonlocal and energy dependent many of the optical spectra for semiconductors can be explained by ignoring this.[1] If we assume the pseudopotential is a simple function of position, then

$$V_p(\vec{r}) = \sum_{\vec{G}} V(\vec{G}) e^{i\vec{G}\cdot\vec{r}}, \tag{3}$$

where

$$V(\vec{G}) = \sum_\alpha S_\alpha(\vec{G}) V_\alpha(\vec{G}),$$

$$S_\alpha(\vec{G}) = \frac{1}{N\alpha} \sum_{\text{cell } j} e^{-i\vec{G}\cdot\vec{R}_j^\alpha}, \tag{4}$$

and

$$V_\alpha(\vec{G}) = \frac{1}{\Omega_a} \int e^{-i\vec{G}\cdot\vec{r}} V_p^a(\vec{r})\, d^3r,$$

where the $\vec{G}$ are reciprocal-lattice vectors and $V_\alpha(\vec{G})$ are the atomic form factors. In this approximation we are assuming the crystalline potential is a sum of local atomic pseudopotentials $V_p^a(\vec{r})$. Ω_a is the atomic volume, N_α is the number of atomic species α present, and $\vec{R}_j^\alpha$ is the position of the jth atom of the αth species. These equations may be specialized in the case of the diamond or zinc-blende compounds, $A^N B^{8-N}$ to

$$V(\vec{G}) = V^S(\vec{G}) \cos(\vec{G}\cdot\vec{\tau}) + iV^A(\vec{G}) \sin(\vec{G}\cdot\vec{\tau}),$$

where

$$V^S(\vec{G}) = \tfrac{1}{2}[V_A(\vec{G}) + V_B(\vec{G})],$$
$$V^A(\vec{G}) = \tfrac{1}{2}[V_A(\vec{G}) - V_B(\vec{G})]. \tag{5}$$

$\tau = \frac{1}{8}a(1,1,1)$, where a is the lattice constant. V^S and V^A are the symmetric and antisymmetric form factors, respectively.

The local empirical pseudopotential method is based upon the above simplification. If we take the pseudopotentials to be spherical so that $V_p^a(\vec{r}) = V_p^a(|\,\vec{r}\,|)$, the form factors depend upon the magnitude of $\vec{G}$, with a corresponding reduction in the number of required form factors. These form factors are the empirically determined parameters fit to experimental data such as optical gaps.

The validity of this approach rests upon two arguments: (i) $E_{\vec{k}} \gg E_t$ so that $(E_{\vec{k}} - E_t)$ can be replaced by a mean energy in (2) such as E_F (providing one is interested in only a limited energy range), and (ii) the cancellation is equal for all l (or at least the l components of the valence wave functions which are significant). Until recently as mentioned in Sec. I, these assumptions have been found to be satisfactory.

If we wish to include the effects of nonlocality or energy dependence we may proceed in a manner discussed extensively elsewhere.[12-16] In order to briefly summarize the method and clarify the notation to be incorporated for the required parameters, we outline the technique below.

We may write a nonlocal (NL) correction term to the local atomic potential term of the form[1]

$$V_{\text{NL}}^a(\vec{r}, E) = \sum_{l=0}^{\infty} A_l(E) f_l(r) \mathcal{P}_l, \tag{6}$$

where $A_l(E)$ is an energy-dependent well depth, $f_l(r)$ is a function simulating the effect of core states with l symmetry, and $\mathcal{P}_l$ is a projection operator for the lth angular momentum component.

Only $l=0$, 1, or 2 components are significant for the case at hand, therefore, we may write (symbolically)

$$s + p + d \simeq 1 \tag{7}$$

TABLE I. Pseudopotential parameters for the diamond-structure semiconductors.

Compound	Form factors (Ry) $V(\sqrt{3})$	$V(\sqrt{8})$	$V(\sqrt{11})$	Lattice constant (Å)
Si [a]	−0.224	0.055	0.072	5.43
Si	−0.257	−0.040	0.033	5.43
Ge	−0.221	0.019	0.056	5.65
α-Sn	−0.190	−0.008	0.040	6.49

Compound	Nonlocal parameters α_0 (Ry)	β_0	A_2 (Ry)	Radii (Å) R_0	R_2
Si	0.55	0.32	0	1.06	0
Ge [b]	0	0	0.275	0	1.22
α-Sn	0	0.40	0.70	1.06	1.41

[a] Purely local pseudopotential.
[b] Gaussian nonlocal well.

and need consider, for example, s and d terms in (6). Model-potential calculations indicate a weak energy dependence for the $A_l(E)$, where $l=1$ or 2.[17]

To choose a form for $f_l(r)$ we employ a square well, a form which has the advantage of simplicity and wide applicability.[1,12] Hence,

$$f_l(r)=\begin{cases}1, & r<R_l,\\ 0, & r\geq R_l.\end{cases} \tag{8}$$

With a plane-wave basis the required matrix elements are of the form

$$V_{\mathrm{NL}}(\vec{K},\vec{K}')=\frac{4\pi}{\Omega_a}\sum_{l,i}A_l^i(E)(2l+1)P_l(\cos(\theta_{KK'}))\times S^i(\vec{K}-\vec{K}')F_l^i(K,K'), \tag{9}$$

where $\vec{K}=\vec{k}+\vec{G}$, $\vec{K}'=\vec{k}+\vec{G}'$, and

$$F_l(K,K')=\begin{cases}(1/2R^2)\{[j_l(KR)]^2-j_{l-1}(KR)j_{l+1}(KR)\}, & K=K',\\ [R^2/(K^2-K'^2)][Kj_{l+1}(KR)j_l(K'R)-K'j_{l+1}(K'R)j_l(KR)], & K\neq K'.\end{cases} \tag{10}$$

The $j_l(x)$ are spherical Bessel functions, $P_l(x)$ are Legendre polynomials, and i is a sum over the atomic species present.[1]

To simulate energy dependence for the s states we make the approximation for the matrix elements between K and K' as follows:

$$A_0(E)=\alpha_0+\beta_0\{[E^0(K)E^0(K')]^{1/2}-E^0(K_F)\}, \tag{11}$$

where $E^0(K)=\hbar^2K^2/2m$. This approximation works quite well compared to more rigorous techniques.[18]

The parameters required by our potential were fixed by detailed comparisons with experimental reflectivity and photoemission data. Unfortunately, the addition of a nonlocal correction term increases the number of parameters rather dramatically. We have attempted to circumvent this by constraining the local part of the pseudopotential to resemble the Cohen-Bergstresser values.[14] The nonlocal radii required were fixed by model potential calculations[17] and by physical considerations. In particular, the s radius was taken from the Heine-Animalu–model calculations,[17] and the d-well radius fixed by "touching spheres" as suggested elsewhere.[12] With the radii thus fixed, the well depths are the only adjustable nonlocal input parameters.

We govern our choice for the nonlocal well depths by inspection of nonlocality in the ion core potential.[17] It is expected that screening could reduce the size of the nonlocality present in the core potential, but the trends are expected to be correct.

B. Band structure

Once the potential is determined, it is a straightforward calculation to solve for the energy-band spectrum. The eigenvalues and eigenvectors are found by solving the secular equation

$$\det|H_{\vec{G},\vec{G}'}(\vec{k})-E(\vec{k})\delta_{\vec{G},\vec{G}'}|=0. \tag{12}$$

For the local approximation, we have

$$H^L_{\vec{G},\vec{G}'}=\frac{\hbar^2}{2m}(\vec{k}+\vec{G})^2\delta_{\vec{G},\vec{G}'}+V(|\vec{G}-\vec{G}'|). \tag{13}$$

The form factors and structure factors are defined as in (5) for diamond and zinc-blende semiconductors.

For nonlocal corrections we may take

$$H^{\mathrm{NL}}_{\vec{G},\vec{G}'}=H^L_{\vec{G},\vec{G}'}+\frac{4\pi}{\Omega_a}\sum_{l\alpha}A_l^\alpha(2l+1)P_l(\cos\theta_{KK'})\times F_l^\alpha(K,K')S^\alpha(\vec{G}-\vec{G}'), \tag{14}$$

where the sum over α refers to the atomic species present. The $F_l(K,K')$ are defined as in (10). An "energy dependence" may be included in the A_l as in (11).

To evaluate the optical response functions or electronic density of states it is necessary to perform a summation over wave vector $\vec{k}$. Thus (12) is solved for a grid of 308 points in the irreducible Brillouin zone.

To achieve satisfactory convergence, typically 50 plane waves are included in the wave-function expansion with another 50 wave treated in an approximate fashion using a scheme due to Löwdin.[1]

C. Optical response functions

The optical spectrum can be calculated as follows. First the imaginary part of the dielectric function is evaluated using the expression[1]

$$\epsilon_2(\omega)=\frac{e^2\hbar^2}{\pi m}\sum_{n_cn_v}\int\frac{f_{n_vn_c}(\vec{k})\,dS}{E_{n_vn_c}(\vec{k})|\nabla_{\vec{k}}E_{n_vn_c}(\vec{k})|}, \tag{15}$$

where

$$E_{n_v n_c}(\vec{k}) = E_{n_c}(\vec{k}) - E_{n_v}(\vec{k})$$

and

$$f_{n_v n_c}(\vec{k}) = \frac{\hbar^2}{m} \frac{|\langle n_c, \vec{k}| \nabla | n_v, \vec{k}\rangle|^2}{E_{n_v n_c}(\vec{k})}$$

is the interband oscillator strength. The sum is over the initial valence-band index n_v and the final conduction-band states n_c. S is a surface in k space of constant interband energy. Four valence bands and six conduction bands were included in the sum. The Gilat-Raubheimer scheme[19] was used to evaluate the integral. The expression for $\epsilon_2(\omega)$ is based upon several assumptions such as neglecting excitonic effects, but has been quite satisfactory for the purpose of analyzing reflectivities.

Once an imaginary part of the dielectric function has been evaluated, the real part and the reflectivity may be calculated from a Kramers-Kronig transformation. To compare the theoretical results to the experimental derivative spectra, the logarithmic derivative of the reflectivity is computed by numerical means.

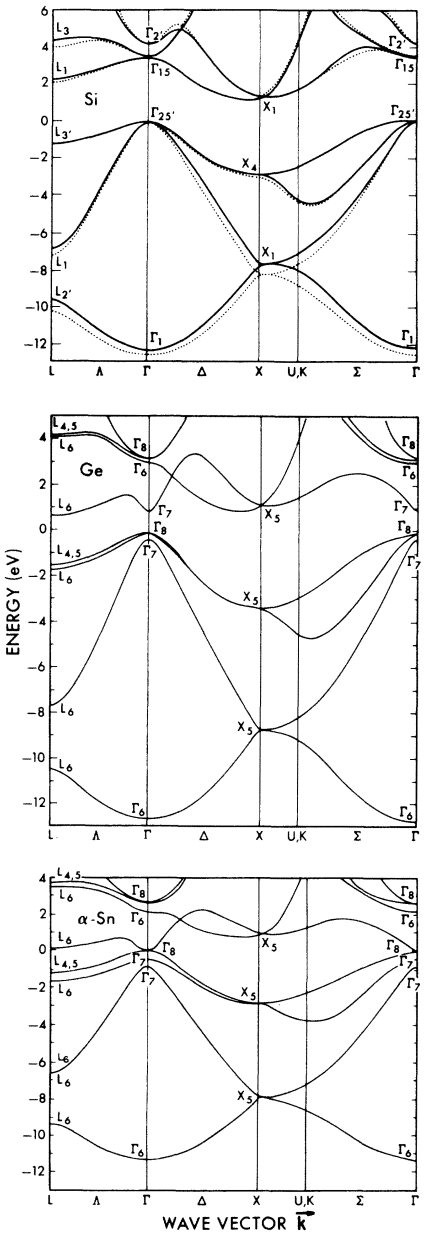

FIG. 1. Band structures for Si, Ge, and α-Sn. In the case of silicon two results are presented: nonlocal pseudopotential (solid line) and local pseudopotential (dashed line).

D. Electronic density of states

The density of states is given by

$$N(E) = \frac{1}{N} \sum_{\vec{k}} \sum_{n} \delta(E - E_n(\vec{k})), \tag{16}$$

where the sum is over wave vector and band index.

TABLE II. Eigenvalues for diamond-structure semiconductors at Γ, X, and L. Energies are in eV.

Point	Level	Si [a]		Compound Ge	Compound α-Sn
		Local	Nonlocal		
Γ	Γ_6^v	−12.53	−12.36	−12.66	−11.34
	Γ_7^v			−0.29	−0.80
	Γ_8^v	0.00	0.00	0.00	0.00
	Γ_7^c	4.17	4.10	0.90	−0.42
	Γ_6^c			3.01	2.08
	Γ_8^c	3.43	3.43	3.22	2.66
X	X_5^v	−8.27	−7.69	−8.65	−7.88
	X_5^v	−2.99	−2.86	−3.29	−2.75
	X_5^c	1.22	1.17	1.16	0.90
L	L_6^v	−10.17	−9.55	−10.39	−9.44
	L_6^v	−7.24	−6.96	−7.61	−6.60
	L_6^v			−1.63	−1.68
	$L_{4,5}^v$	−1.22	−1.23	−1.43	−1.20
	L_6^c	2.15	2.23	0.76	0.14
	L_6^c			4.16	3.48
	$L_{4,5}^c$	4.00	4.34	4.25	3.77

[a] Spin-orbit corrections not included.

The energy gradients required (Ref. 19) were calculated from $\vec{k}\cdot\vec{p}$ perturbation theory.

E. Pseudocharge density

The pseudocharge density was calculated by using the special point scheme of Chadi and Cohen.[20] Instead of evaluating the sum[21]

$$\rho(\vec{r}) = e\sum_{\vec{k}}\sum_{n_v} |\psi_{n_v,\vec{k}}(\vec{r})|^2 \tag{17}$$

over a fine grid throughout the Brillouin zone as performed by Walter and Cohen,[22] only a few representative points need be considered. The two-point scheme of Chadi and Cohen, with $\vec{k}_1 = (2\pi/a)(\frac{1}{4},\frac{1}{4},\frac{1}{4})$ and $\vec{k}_2 = (2\pi/a)(\frac{3}{4},\frac{1}{4},\frac{1}{4})$ yields a valence-band pseudocharge density accurate to within (1–2)%,[23] as compared to a sum throughout the zone. Approximately 90 plane waves were used in the calculation of the required pseudo-wave-functions.

F. Spin-orbit interactions

For the heavier elements the atomic spin-orbit splittings become rather large. An example is CdTe where the energy bands split by nearly 1 eV at the valence-band maximum. Since we are interested in obtaining precise band structures such interactions must be considered.

We have included spin-orbit interactions by extension of a method first presented by Saravia and Brust[24] for Ge. Following the work of Weisz,[25] as modified by Bloom and Bergstresser,[26] we may write the spin-orbit matrix element contribution

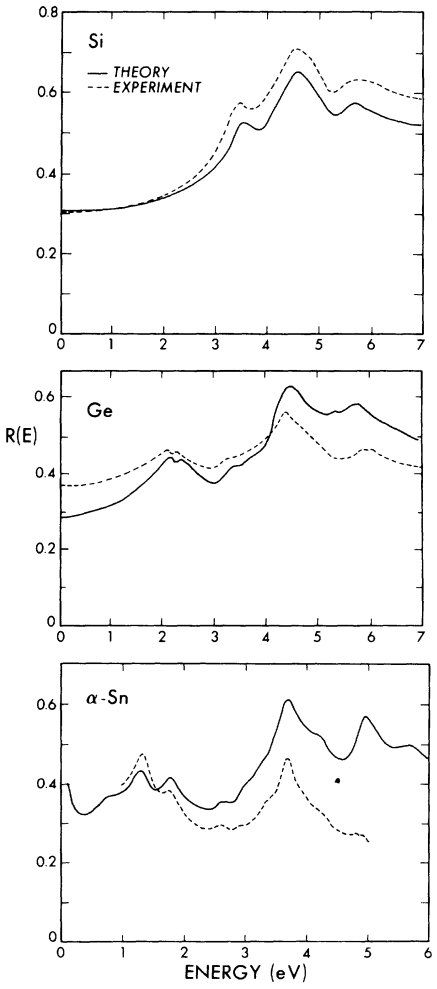

FIG. 2. Theoretical and experimental reflectivity spectra for Si, Ge, and α-Sn. The experimental results are from Ref. 30 for Si and Ge and Ref. 31 for α-Sn.

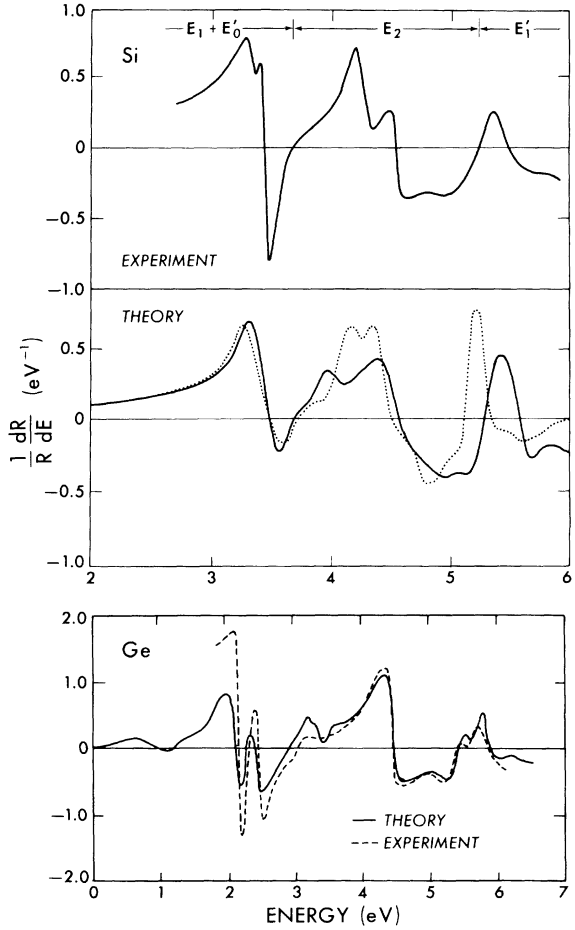

FIG. 3. Calculated derivative reflectivity spectra for Si and Ge compared to experiment. The experimental results are from Ref. 32 and Ref. 33, respectively. In the case of Si two results are displayed: nonlocal pseudopotential (solid line) and local pseudopotential (dotted line).

TABLE III. Theoretical and experimental reflectivity structure and their identifications including location in the Brillouin zone, energy (in eV) and symmetry of the calculated critical points for Si.

Si Reflectivity structure Theory Local	Theory Nonlocal	Experiment 5 °K [a]	Experiment 80 °K [b]	Associated critical points (cp) location in the Brillouin zone Local	Nonlocal	Symmetry of CP Local	Nonlocal	Critical-point energy Local	Nonlocal
3.48	3.49	3.40	3.36	$L_{3'}$-L_1	$L_{3'}$-L	M_0	M_0	3.37	3.46
		3.45	3.41	$\Gamma_{25'}$-Γ_{15}	$\Gamma_{25'}$-Γ_{15}	M_0	M_0	3.43	3.42
				Near (0.1, 0.02, 0.02)	Near (0.1, 0.05, 0.05)	M_0	M_0	3.46	3.42
3.75	3.70	3.66	(3.88) [c]	Vol. along Δ	Vol. along Δ	...	...	...	...
4.26	4.15	4.30	4.38	Vol. near (0.9, 0.1, 0.1)	Vol. near (0.9, 0.1, 0.1)	...	...	...	...
4.53	4.57	4.57	4.57	Large region near (0.5, 0.25, 0.25) and	Large region near (0.6, 0.3, 0.3) and	M_2	M_2	4.53	4.47
				Σ_4-Σ_1	Σ_4-Σ_1	M_2	M_2	4.49	4.60
5.32	5.58	5.48	...	L_3-$L_{3'}$	L_3-$L_{3'}$	M_0	M_2	5.22	5.56
				Λ_3-$\Lambda_{3'}$ (0.4, 0.4, 0.4)	Λ_3-$\Lambda_{3'}$ (0.45, 0.45, 0.45)	M_1	~M_3	5.25	5.57

[a] From Ref. 32.
[b] From Ref. 34.
[c] Inferred from $\epsilon_2(\omega)$ data of Ref. 34.

to the pseudopotential Hamiltonian as

$$H^{so}_{\vec{G},\vec{G}'}(\vec{k}) = (\vec{K}\times\vec{K}')\cdot\vec{\sigma}_{s,s'}\{-i\lambda^s\cos[(\vec{G}-\vec{G}')\cdot\vec{\tau}] + \lambda^A\sin[(\vec{G}-\vec{G}')\cdot\vec{\tau}]\}, \quad (18)$$

where we define

$$\lambda^s = \tfrac{1}{2}(\lambda_A+\lambda_B), \quad \lambda^A = \tfrac{1}{2}(\lambda_A-\lambda_B),$$
$$\lambda_A = \mu B^A_{nl}(K)B^A_{nl}(K'),$$
$$\lambda_B = \alpha\mu B^B_{nl}(K)B^B_{nl}(K').$$

TABLE IV. Theoretical and experimental reflectivity structure at 5 °K for Ge (from Ref. 33), and their identifications, including the location in the Brillouin zone, energy, and symmetry of the calculated critical points.

Ge Reflectivity structure (eV) Theory	Experiment	Associated critical points, location in zone	Symmetry	Critical-point energy (eV)
2.20	2.22	L^v_6-L^c_6 (0.5, 0.5, 0.5)	M_1	2.19
2.40	2.42	$L^v_{4,5}$-L^v_6	M_1	2.39
3.3	3.20	Γ^v_{25}-Γ^c_{15} complex (0.0, 0.0, 0.0)	M_0	3.25
4.51	4.5	Region near (0.75, 0.25, 0.25)	...	...
5.40	5.65	Δ^v_6-Δ^c_6 (0.5, 0.0, 0.0)	M_1	5.40
		Δ^v_7-Δ^c_6		5.35
5.88	5.88	$L^v_{4,5}$-$L^c_{4,5}$ (0.5, 0.5, 0.5)	M_1	5.88
		L^v_6-L^c_6	M_1	5.60

TABLE V. Theoretical and experimental reflectivity structure for α-Sn and their identifications, including the location in the Brillouin zone, energy, and symmetry of the calculated critical points.

α-Sn Reflectivity structure (eV) Theory	Experiment (a)	Experiment (b)	Associated critical points, location in zone	Symmetry	Critical-point energy (eV)
1.34	1.365	1.365	L_6^v-$L_{4,5}^c$ (0.5, 0.5, 0.5)	M_1	1.34
1.83	1.832	1.845	L_6^v-L_6^c	M_1	1.83
2.31	...	2.28	Γ_8^v-Γ_6^c (0.0, 0.0, 0.0)	M_0	2.08
2.67	2.62	2.63	Γ_8^v-Γ_8^c	M_0	2.66
2.95	2.85	...	Δ_7^v-Δ_6^c (0.2, 0.0, 0.0)	M_1	2.91
3.40	3.3	3.3	Γ_7^v-Γ_8^c	M_0	3.46
3.78	3.75	3.718	Plateau near (0.75, 0.25, 0.25)	...	...
4.2	4.0	4.12	Δ_6^v-Δ_7^c (0.6, 0.0, 0.0)	M_1	4.13
4.31	4.43	4.43	Δ_7^v-Δ_7^c	M_1	4.25
4.91	4.89	4.89	$L_{4,5}^v$-L_6^c	M_1	4.68

[a] Reflectivity measurement from Ref. 31.
[b] Electroreflectance measurement from Ref. 35.

σ are the Pauli spin states and λ^s, λ^A are the symmetric and antisymmetric contributions to the spin-orbit Hamiltonian. μ is an adjustable parameter, and α is constrained such that the ratio of the spin-orbit contributions for the atoms A and B are the same as the spin-orbit splitting ratio for free atoms.[27]

The B_n are defined by

$$B_{nl}(K) = \beta \int_0^\infty j_{nl}(Kr) R_{nl}(r) r^2 \, dr ,$$

where R_{nl} is the radial part of core wave function. β is a normalization constant as in Ref. 27. The radial wave functions are taken from the Herman-Skillman tables.[28]

We only include contributions from the outermost p-core states. Contributions from inner core states or d-core states may be neglected.[26,27]

In the Saravia-Brust-method[24] spin-orbit interactions are treated by perturbation theory. If at some wave vector $\vec{k}$ we have bands n and m such that

$$|E_n(\vec{k}) - E_m(\vec{k})| < E_0 ,$$

then these bands are treated as "degenerate" and degenerate perturbation theory is used to include the spin-orbit correction. Otherwise nondegenerate perturbation theory is used.

In the degenerate perturbation technique we must solve

$$\det | H_{mn}^{ss'}(\vec{k}) - E(\vec{k}) \delta_{ss'} \delta_{mn} | = 0 , \tag{19}$$

where

$$H_{mn}^{ss'}(\vec{k}) = \sum_{\vec{G},\vec{G}'} \alpha_{\vec{G}}^{m}(\vec{k}) \alpha_{\vec{G}'}^{n}(\vec{k}) H_{\vec{G},\vec{G}'}^{so}(\vec{k}) + E_m(\vec{k}) \delta_{m,n} \delta_{ss'} . \tag{20}$$

$E_m(\vec{k})$ is the band energy without spin orbit, H^{so} is given by (18), and the pseudo-wave-functions by

$$\psi_{\vec{k}}^{m}(\vec{r}) = \sum_{\vec{G}} \alpha_{\vec{G}}^{m}(\vec{k}) e^{i(\vec{k}+\vec{G})\cdot\vec{r}} .$$

E_0 is chosen such that it is large compared to the spin-orbit splitting. By a direct comparison with calculations which include spin orbit exactly, it is found $E_0 \approx 2$ eV is quite satisfactory for the case at hand. Even with rather large spin-orbit splittings (e.g., 1 eV), the perturbation technique is accurate to within 5% and reduces the computational time typically by almost an order of magnitude.

III. RESULTS

The results of our pseudopotential calculations are presented in this section for 11 diamond and zinc-blende crystals. We include results for Ge, GaAs, and ZnSe for completeness although the method we used for these crystals differs slightly from the technique described above.[29]

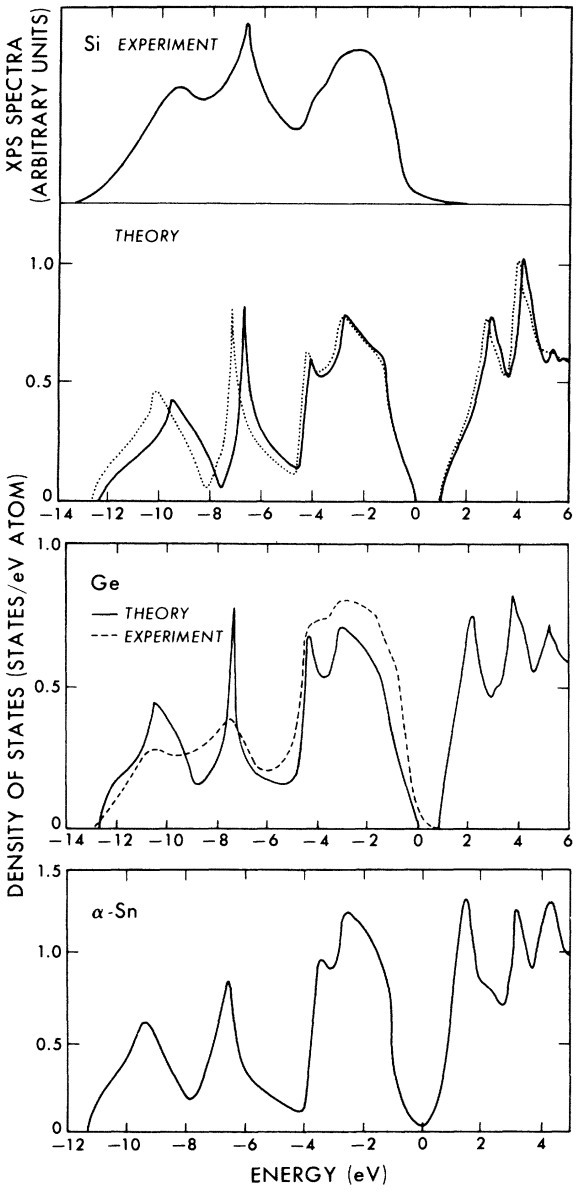

FIG. 4. Calculated electronic densities of states compared to experiment for Si, Ge, and α-Sn. The experimental results for Si and Ge are from Refs. 2 and 3, respectively. In the case of Si two results are displayed: nonlocal pseudopotential (solid line) and local pseudopotential (dashed line).

A. Diamond-structure semiconductors

In this subsection we shall discuss the diamond structure semiconductors: Si, Ge, and α-Sn. Results for Si have been presented elsewhere[15] and are summarized below. The parameters used in the calculations for these crystals are listed in Table I. Si was examined with both a local and nonlocal potential. The nonlocal potential was required to alter the bonding charge and obtain agreement with recent x-ray experimental data.[9] This type of information was not considered in the case of Ge or α-Sn, therefore, a comparison between nonlocal terms is not appropriate.

Spin-orbit interactions were considered in Ge and α-Sn, but not in Si where they are negligible (e.g., $\Delta_0 \approx 0.05$ eV). The spin-orbit parameters μ are 0.000 97 and 0.002 25 for Ge and α-Sn, respectively.

The band structure for the three diamond semiconductors is given in Fig. 1. The most striking feature of the three band structures is the ordering of the first two conduction bands. In Si the lowest-lying conduction band at Γ, Γ_{15}, is p-like; however, in Ge and α-Sn the s-like $\Gamma_{2'}$ band is the lowest conduction band. A related effect is the decrease in the optical gap of Si from 3.4 eV to identically zero is the semimetallic α-Sn. This trend can be understood in chemical terms as arising from an increase in the promotion energy for the creation of sp^3 orbitals in going from Si to α-Sn.[1]

The energy eigenvalues at Γ, X, and L for the valence bands and first few conduction bands are given in Table II.

In Fig. 2 the reflectivity spectra are presented. With the exception of the magnitude of the experimental and theoretical reflectivities, especially for energies larger than the most prominent (E_2) peak, the agreement is quite good. Modulated reflectivity spectra, which are a more sensitive test, are given in Fig. 3 for Si and Ge. An equivalent experimental curve for α-Sn is not available. The experimental reflectivity spectra were taken at room temperature while the derivative spectra were taken at lower temperatures (i.e., 5°K). This accounts for the small shifts in peak positions between Figs. 2 and 3.

In Tables III–V the major reflectivity structure is identified and associated with Van Hove singularities (or critical points) in the joint density of states.[1] For Si numerous critical points are known to exist for the leading absorption edge, and a precise ordering of the energy levels is still in question.[15] A major result in Ge and α-Sn is the effect of the nonlocal pseudopotential on critical point symmetries and location in the Brillouin zone.[7,8] For example, in Ge the local pseudopo-

TABLE VI. Calculated valence-band electronic densities of states for diamond-structure semiconductors compared to experiment.

Feature	Compound: Si Theory Local	Si Theory Nonlocal	Si Experiment	Ge Theory	Ge Experiment	α-Sn Theory
Γ_1	−12.4	−12.5	−12.4 ± 0.6 [a] −12.5 ± 0.6 [b]	−12.6	−12.6 ± 0.3 [a] −12.8 ± 0.4 [b]	−11.3
L_2	−10.2	−9.5	−9.3 ± 0.4 [b]	−10.3	−10.6 ± 0.4 [a] −10.5 ± 0.4 [b]	−9.4
L_1	−7.2	−6.9	−6.4 ± 0.4 [a] −6.8 ± 0.2 [b]	−7.5	−7.7 ± 0.2 [a] −7.4 ± 0.2 [b]	−6.6
$\Sigma_1^{\min}$	−4.5	−4.5	−4.4 [c] −4.7 ± 0.3 [a,b]	−4.6	−4.5 ± 0.2 [a] −4.5 ± 0.2 [b]	−3.3
L_3'	−1.2	−1.2	−1.2 ± 0.2 [c]	−1.4	−1.4 ± 0.2 [c]	−1.2

[a] See Refs. 3 and 6.
[b] See Refs. 2 and 5.
[c] See Ref. 38.

tential yields an M_0 critical point for $L_1 - L_3'$ and an M_1 critical point midway between Γ and L.[8] The nonlocal potential displaces the M_1 critical point to the zone edge, thus eliminating the M_0 critical point. Experimentally the nonlocal result is favored.[8,36] Another result of the nonlocal pseudopotential is the creation of a strong critical point near the special point $(\frac{3}{4}, \frac{1}{4}, \frac{1}{4})$.[7] This region is dominant in producing the E_2 reflectivity peak: a result suggested by recent modulated reflectivity measurements.[7,36]

A comparison of the optical spectra indicates a striking similarity (especially considering that the conduction band structure is quite different). The principal difference between the spectra, a shifting of analogous structure to lower energies from Si to α-Sn, occurs because of the increase in metallicity.

In Fig. 4 the electronic densities of states are displayed and compared to the results of[2,5] XPS and[3,6] UPS for the case of Si and Ge, respectively. Unfortunately, a UPS or XPS spectrum for α-Sn does not exist. However, a comparison between a recent orthogonalized-plane-wave calculation[37] and the nonlocal pseudopotential for α-Sn yields good agreement. Unlike the conduction band structure the electronic density of states for Si, Ge, and α-Sn remains nearly constant. The various structures observed in the experimental spectra are identified and compared with the theoretical results in Table VI. The agreement between theory and experiment is quite good.

Valence charge densities for Si, Ge, and α-Sn have been calculated. Comparisons with experiment has ascertained that nonlocal pseudopotentials can yield accurate bonding charge distributions.[9] In Fig. 5 the valence charge density as calculated using experimental data is compared to the nonlocal pseudopotential results. The

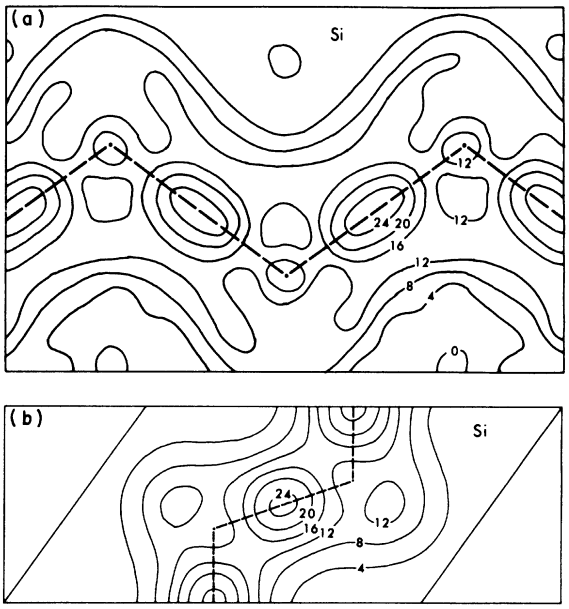

FIG. 5. Valence charge density as determined by Yang and Coppens (Ref. 9) from x-ray experimental data. (b) Valence charge density as calculated by a nonlocal pseudopotential. In both cases the contours are in units of e/Ω_c.

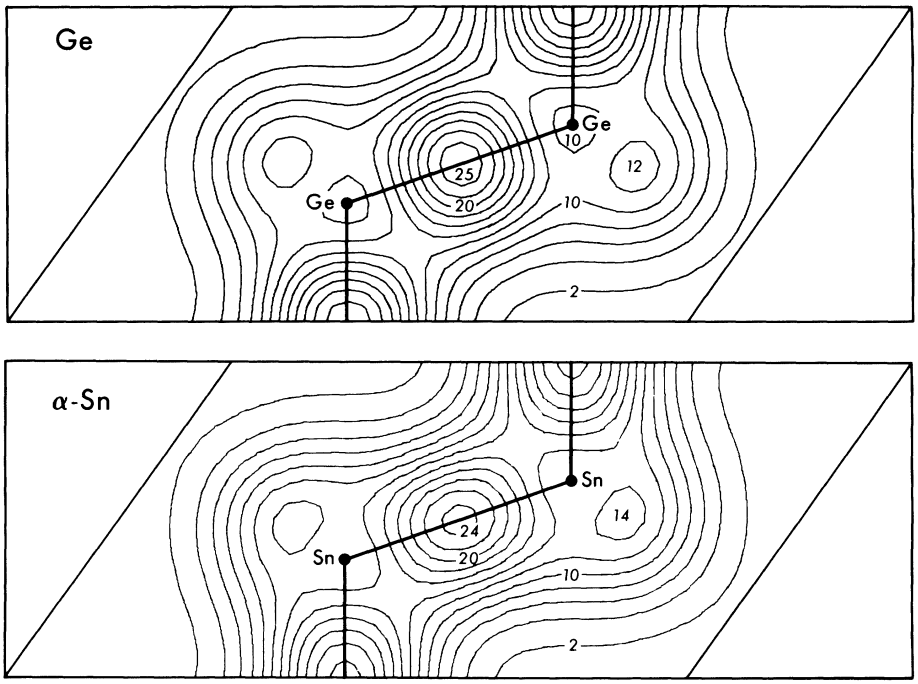

FIG. 6. Calculated valence charge densities for Ge and α-Sn. The contours are in units of e/Ω_c.

local pseudopotential calculation produces a bond oriented perpendicular to the bonding direction.[15] In Fig. 6 the calculated charge densities for Ge and α-Sn are displayed. The bonding charge maximum in units of e/Ω_c are almost identical in Ge and α-Sn. However, Ge has a slightly more localized bond as to be expected since it is more covalent than α-Sn. In Table VII the Fourier coefficients of the valence charge densities are given. If Hartree-Fock wave functions are used to include the core charge densities, these coefficients may be used to calculate the x-ray structure factors.

B. III-V zinc-blende semiconductors

In this subsection we shall discuss six zinc-blende semiconductors: GaP, GaAs, GaSb, InP, InAs, and InSb. The parameters used in the calculation are given in Table VIII. Spin-orbit interactions were not included for GaP because of their negligible size. For the cations α_0 was constrained to be identically zero, and the model radii[17] R_0, 1.27 and 1.06 Å were used for the cations and anions, respectively. The band structures are given in Fig. 7 for the Ga compounds and in Fig. 8 for the In compounds. As expected in both cases the optical gap decreases with the heavier anion. As an example in GaP the optical gap is 2.9 eV and in GaSb the gap is 0.9 eV. A cross comparison with the In compounds shows the gap also decreases with a heavier cation. As an example, the gap is 1.51 eV for GaAs and 0.37 eV in InAs. Considerable effort has been spent in interpreting trends in the optical gaps in terms of the chemical bonding and ionicity of the crystal.[39] Following the pattern of spin-orbit interactions in the free atoms, the spin-orbit splitting at the valence-band maximum increases with the heavier elements. The eigenvalues at Γ, X, and L are given in Table IX.

The reflectivity spectra are given in Fig. 9 for the Ga compounds and Fig. 10 for the In compounds. The corresponding modulated reflec-

TABLE VII. Fourier coefficients of the valence charge densities for diamond-structure semiconductors. The origin for this calculation is at the bond site.

	Fourier coefficients ($e/\Omega c$) Compound			
	Si			
$\vec{G}(a/2\pi)$	Local	Nonlocal	Ge	α-Sn
(000)	8.000	8.000	8.000	8.000
(111)	−1.748	−1.924	−1.807	−1.956
(220)	0.270	0.035	0.109	−0.098
(311)	0.412	0.345	0.373	0.262
(222)	0.481	0.467	0.466	0.364
(400)	0.206	0.273	0.243	0.223
(331)	0.018	0.015	0.025	0.011

TABLE VIII. Pseudopotential parameters for the III-V zinc-blende semiconductors. α_0 and A_2 are in Ry.

Compound	Form factors (Ry) $V^S(\sqrt{3})$	$V^S(\sqrt{8})$	$V^S(\sqrt{11})$	$V^A(\sqrt{3})$	$V^A(\sqrt{4})$	$V^A(\sqrt{11})$	Lattice constant (Å)
GaP	−0.230	0.020	0.057	0.100	0.070	0.025	5.45
GaAs	−0.214	0.014	0.067	0.055	0.038	0.001	5.65
GaSb	−0.220	0.005	0.045	0.040	0.030	0.000	6.10
InP	−0.235	0.000	0.053	0.080	0.060	0.030	5.86
InAs	−0.230	0.000	0.045	0.055	0.045	0.010	6.05
InSb	−0.200	−0.010	0.044	0.044	0.030	0.015	6.47

	Nonlocal parameters					
	Cation			Anion		Spin orbit
Compound	β_0	A_2	α_0	β_0	A_2	μ
GaP	0.30	0.40	0.32	0.05	0.45	...
GaAs [a]	0	0.125	0	0	0.625	0.000 80
GaSb	0.20	0.20	0	0.30	0.60	0.0011
InP	0.25	0.55	0.30	0.05	0.35	0.0020
InAs	0.35	0.50	0	0.25	1.00	0.0012
InSb	0.45	0.55	0	0.48	0.70	0.0018

[a] Gaussian nonlocal well.

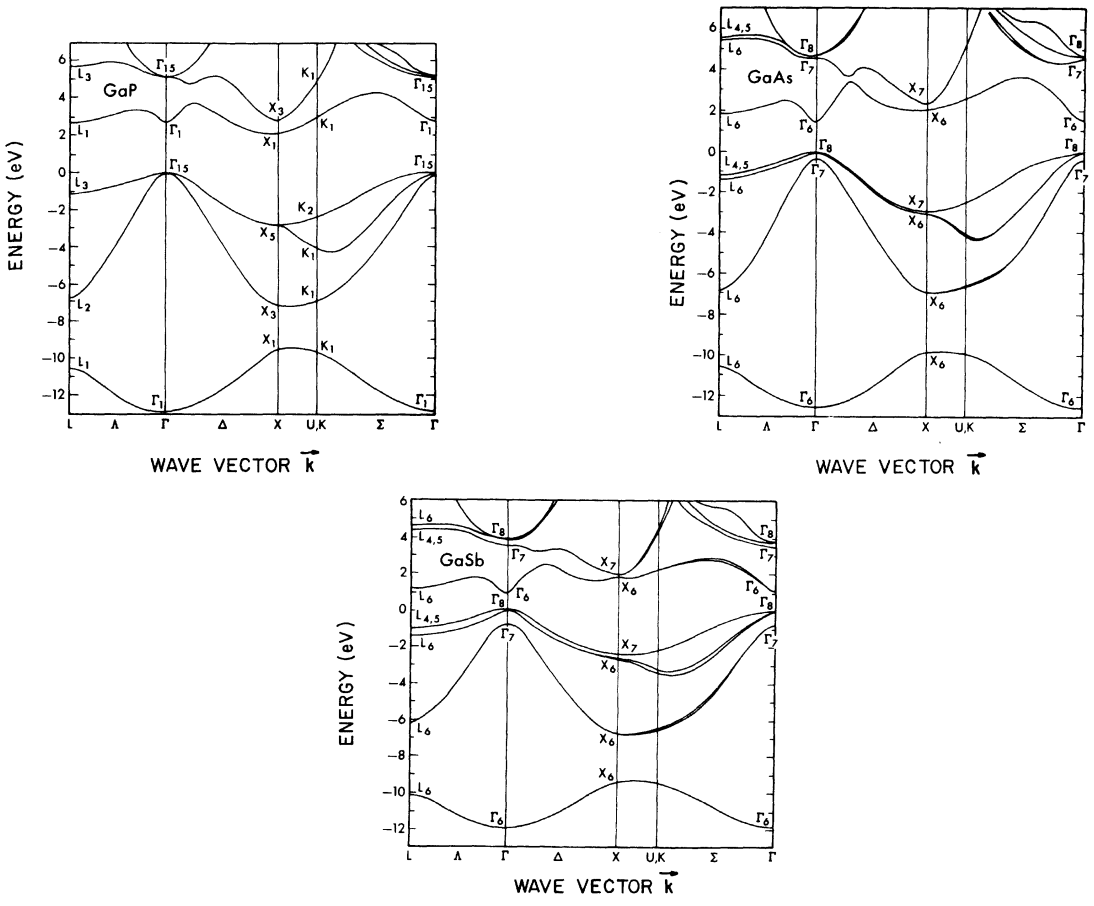

FIG. 7. Band structures for GaP, GaAs, and GaSb.

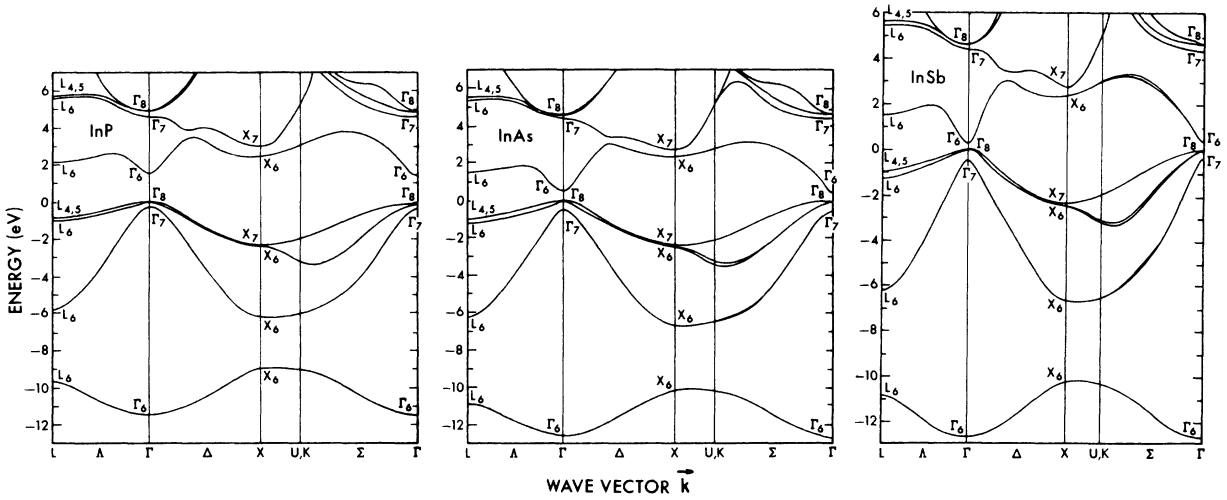

FIG. 8. Band structures for InP, InAs, and InSb.

TABLE IX. Eigenvalues at Γ, X, and L for III-V zinc-blende semiconductors. Energies are in eV.

Point	Level	Compound					
		GaP [a]	GaAs	GaSb	InP	InAs	InSb
Γ	Γ_6^v	−12.99	−12.55	−12.00	−11.42	−12.69	−11.71
	Γ_7^v		−0.35	−0.76	−0.21	−0.43	−0.82
	Γ_8^v	0.00	0.00	0.00	0.00	0.00	0.00
	Γ_6^c	2.88	1.51	0.86	1.50	0.37	0.25
	Γ_7^c		4.55	3.44	4.64	4.39	3.16
	Γ_8^c	5.24	4.71	3.77	4.92	4.63	3.59
X	X_6^v	−9.46	−9.83	−9.33	−8.91	−10.20	−9.20
	X_6^v	−7.07	−6.88	−6.76	−6.01	−6.64	−6.43
	X_6^v		−2.99	−2.61	−2.09	−2.47	−2.45
	X_7^v	−2.73	−2.89	−2.37	−2.06	−2.37	−2.24
	X_6^c	2.16	2.03	1.72	2.44	2.28	1.71
	X_7^c	2.71	2.38	1.79	2.97	2.66	1.83
L	L_6^v	−10.60	−10.60	−10.17	−9.67	−10.92	−9.95
	L_6^v	−6.84	−6.83	−6.25	−5.84	−6.23	−5.92
	L_6^v		−1.42	−1.45	−1.09	−1.26	−1.44
	$L_{4,5}^v$	−1.10	−1.20	−1.00	−0.94	−1.00	−0.96
	L_6^c	2.79	1.82	1.22	2.19	1.53	1.03
	L_6^c		5.47	4.43	5.58	5.42	4.30
	$L_{4,5}^c$	5.74	5.52	4.59	5.70	5.55	4.53

[a] Spin-orbit interactions not included.

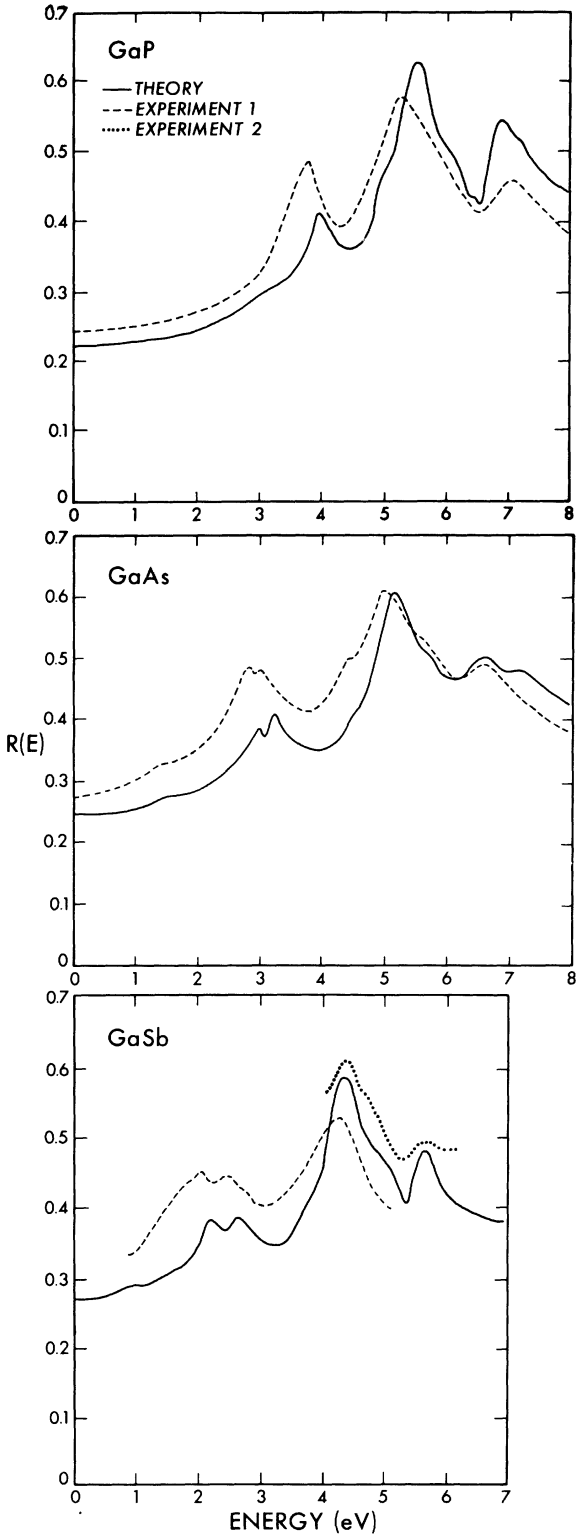

FIG. 9. Calculated reflectivity spectra for GaP, GaAs, and GaSb compared to experiment. For GaP and GaAs the experimental results are from Ref. 30. For GaSb the dashed line is from Ref. 40 and the dotted line is from Ref. 41.

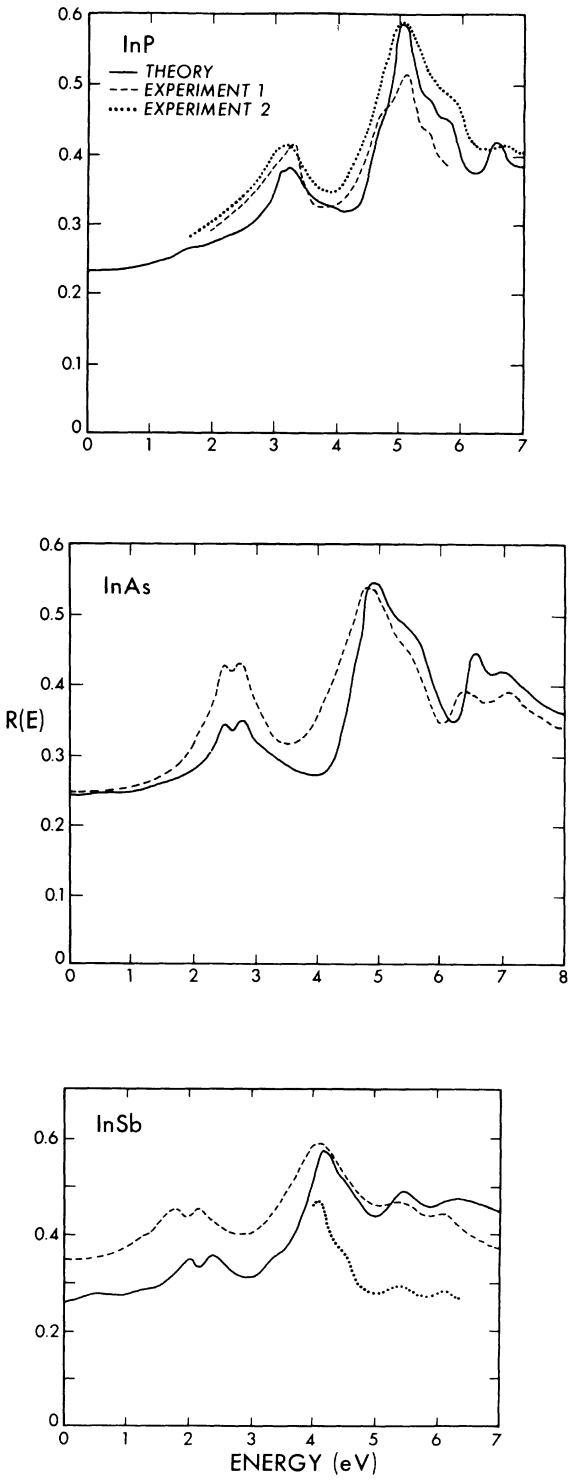

FIG. 10. Calculated reflectivity spectra for InP, InAs, and InSb compared to experiment. For InP the experimental results are from Ref. 42 (dotted line) and Ref. 43 (dashed line). For InSb the experimental results are from Ref. 44 (dashed line) and Ref. 40 (dotted line). For InAs the experimental results are from Ref. 30.

tivities are given in Figs. 11 and 12. The prominent reflectivity structure is identified and compared to experiment in Tables X–XV. The structure for all of the III-V compounds can be decomposed, as true of the diamond semiconductors, into five distinct regions: E_0, E_1, E_0', E_2, and E_1'.[1] The lowest-energy region E_0 is dominated by structure originating from the fundamental optical gap at Γ. Structure in this region is not prominent because of the small phase space occurring at Γ. The E_1 peak originates from transitions occurring near or at L. The line shape of this structure has been modified strongly by the nonlocal pseudopotential; the M_1 critical point occurring at L for local pseudopotentials has been eliminated. The E_0' structure can arise from either of two regions: near Γ or along the Δ direction. Recent work by Aspnes and Studna has given support to the Γ transition.[46] The Γ region has not been considered of major importance because of its small phase space.[1] However, excitonic effects could enhance its contribution in the experimental spectra. The E_2 peak arises from a well-defined plateau region near the special point $(\frac{3}{4}, \frac{1}{4}, \frac{1}{4})$.[7] The transitions in this region dominate the spectra because of the large phase space and strong matrix elements. Following the E_2 peak, structure arising from Δ transitions is often present. The E_1' structures arises from transitions from the top valence band to the second

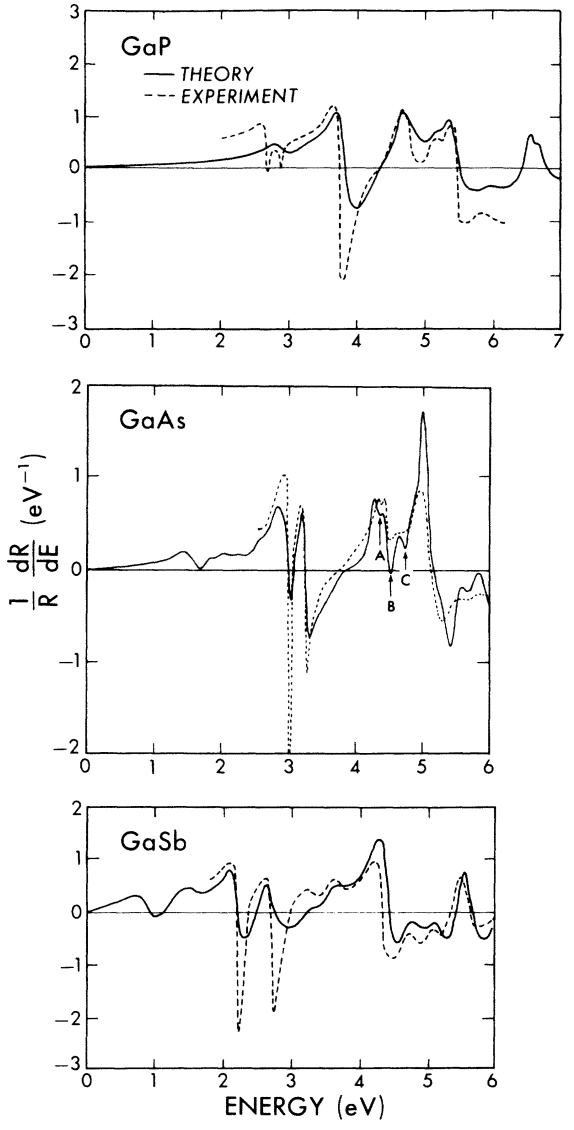

FIG. 11. Calculated derivative reflectivity spectra for GaP, GaAs, and GaSb compared to experiment. The experimental results are from Ref. 42 for GaP, and Ref. 33 for GaAs and GaSb. For a discussion of the fine structure in GaAs, labeled by A, B, C, see Ref. 13.

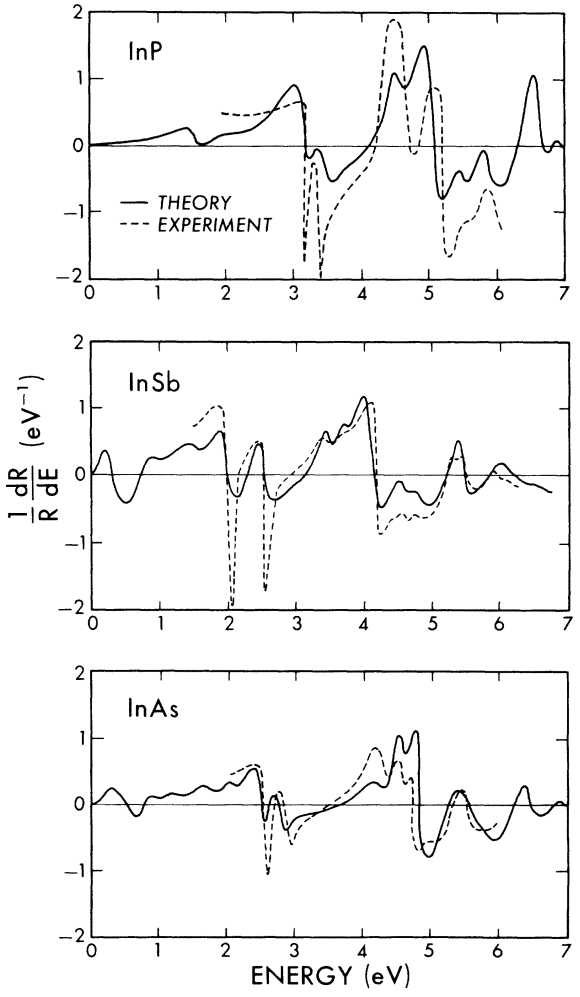

FIG. 12. Calculated derivative reflectivity spectra for InP, InAs, and InSb. The experimental results are from Ref. 42 for InP and Ref. 33 for InAs and InSb.

TABLE X. Identification of transitions responsible for the prominent theoretical and experimental reflectivity structure in GaP, including location in the Brillouin zone, energy, and symmetry for calculated critical points. The experimental results are from Ref. 42 for 5 °K.

GaP Reflectivity structure (eV) Theory	Experiment	Location in Brillouin zone	Symmetry	Critical energy (eV)
2.95	2.89 [a] 2.97	Γ_{15}^{v}- Γ_{1}^{c} (0.0, 0.0, 0.0)	M_0	2.88
3.89	3.79	L_{3}^{v}-L_{1}^{c} (0.5, 0.5, 0.5)	M_1	3.89
4.95	4.80	Δ_{5}^{v}-Δ_{1}^{c} (0.7, 0.0, 0)	M_1	4.91
5.24	5.19	Γ_{15}^{v}- Γ_{15}^{c} (0.0, 0.0, 0.0)	···	5.24
5.45	5.42	Plateau near (0.6, 0.2, 0.2)	···	
6.8	6.7 [b]	L_{3}^{v}-L_{3}^{c} (0.5, 0.5, 0.5)	M_1	6.84

[a] Spin-orbit splitting (not included in the calculation).
[b] From Ref. 45.

conduction band at L. One of the effects of the d well is to increase the energy of the E_1' peak position and also the E_2 peak. As discussed elsewhere the main deficiency of reflectivities described by local pseudopotentials is the underestimation of the optical gaps.[12]

While a comparison of the calculated and experimental reflectivities yields good agreement, one noticeable discrepancy occurs in all cases. This is the relative strength of the reflectivity peaks. In GaAs the effect is quite apparent. At energies below the E_2 peak, the theoretical reflectivity is consider-

TABLE XI. Theoretical and experimental reflectivity structure for GaAs at 5 °K (from Ref. 33), and their identifications, including the location in the Brillouin zone, energy, and symmetry of the calculated critical points.

GaAs Reflectivity structure (eV) Theory	Experiment	Associated critical points, location in zone	Symmetry	Critical-point energy (eV)
3.03	3.02	$L_{4,5}^{v}$-L_{6}^{c} (0.5, 0.5, 0.5)	M_1	3.03
3.25	3.25	L_{6}^{v}-L_{6}^{c}	M_1	3.25
4.55	4.44	Δ_{5}^{v}-Δ_{5}^{c} (0.1, 0.0, 0.0)	M_1	4.54
4.70	4.64	Δ_{5}^{v}-Δ_{5}^{c}		4.70
5.13	5.11	Plateau near (0.75, 0.25, 0.25)	···	5.07
5.59	5.64	X_{7}^{v}-X_{7}^{c} (1.0, 0.0, 0.0)	M_0	5.28
		X_{6}^{v}-X_{7}^{c}		
5.84	5.91	Δ_{5}^{v}-Δ_{5}^{c} (0.55, 0.0, 0.0)	M_1	5.76
6.7	6.6 [a]	$L_{4,5}^{v}$-$L_{4,5}^{c}$	M_1	6.67
		$L_{4,5}^{v}$-$L_{4,5}^{c}$		6.74

[a] From Ref. 30.

TABLE XII. Identification of transitions responsible for the prominent theoretical and experimental reflectivity structure in GaSb, including location in the Brillouin zone, energy, and symmetry of calculated critical points. The experimental results are from Ref. 33.

GaSb Reflectivity structure (eV)				
Theory	Experiment	Location in Brillouin zone	Symmetry	Critical-point energy (eV)
2.22	2.15	$L_{4,5}^{v}$-L_{6}^{c} (0.5, 0.5, 0.5)	M_1	2.22
2.86	2.60	L_{6}^{v}-L_{6}^{c}	M_1	2.67
3.3	3.35	Γ_{8}^{v}- Γ_{7}^{c} (0.0, 0.0, 0.0)	M_0	3.44
3.76	3.69	Γ_{8}^{v}- Γ_{8}^{c} (0.0, 0.0, 0.0)	M_0	3.77
4.37	4.35	Plateau near (0.7, 0.2, 0.2)	...	
4.84	4.75	Δ_{5}^{v}-Δ_{5}^{c} (0.6, 0.0, 0.0)	M_1	4.84
5.13	5.07	Δ_{5}^{v}-Δ_{5}^{c}	M_1	5.12
5.65	5.65	$L_{4,5}^{v}$-L_{6}^{c} (0.5, 0.5, 0.5)	M_1	5.43

TABLE XIII. Identification of transitions responsible for the prominent theoretical and experimental reflectivity structure in InP, including location in the Brillouin zone, energy, and symmetry of calculated critical points. The experimental results are from Ref. 42 (except as noted).

InP Reflectivity structure (eV)				
Theory	Experiment	Location in Brillouin zone	Symmetry	Critical-point energy (eV)
1.50	1.42	Γ_{8}^{v}- Γ_{6}^{c} (0.0, 0.0, 0.0)	M_0	1.50
3.13	3.24	$L_{4,5}^{v}$-L_{6}^{c} (0.5, 0.5, 0.5)	M_1	3.13
3.28	3.38	L_{6}^{v}-L_{6}^{c}		3.28
4.76	4.78	Γ_{8}^{v}- Γ_{7}^{c} (0.0, 0.0, 0.0)	M_0	4.64
		Δ_{5}^{v}-Δ_{5}^{c} (0.2, 0.0, 0.0)	M_1	4.80
5.05	5.10	Plateau near (0.75, 0.25, 0.25)	...	5.00
5.44	5.25 [a]	Γ_{7}^{v}- Γ_{8}^{c} (0.0, 0.0, 0.0)	M_0	5.13
5.73	5.77	Δ_{5}^{v}-Δ_{5}^{c} (0.7, 0.0, 0.0)	M_1	5.62
6.55	6.57 [a]	$L_{4,5}^{v}$-L_{6}^{c} (0.5, 0.5, 0.5)	M_1	6.52

[a] From Ref. 40.

TABLE XIV. Identification of transitions responsible for the prominent theoretical and experimental reflectivity structure in InAs, including location in the Brillouin zone, energy, and symmetry of calculated critical points. The experimental results are from Ref. 33 (except as noted).

InAs Reflectivity structure (eV)		Location in		Critical-point energy
Theory	Experiment	Brillouin zone	Symmetry	(eV)
2.54	2.61	$L_{4,5}^{v}$-L_{6}^{c} (0.5, 0.5, 0.5)	M_1	2.53
2.81	2.88	L_{6}^{v}-L_{6}^{c}	M_1	2.79
4.3	4.39	Γ_{8}^{v}- Γ_{7}^{c} (0.0, 0.0, 0.0)	M_0	4.39
4.52	4.58	Γ_{8}^{v}- Γ_{8}^{c}	M_0	4.63
4.85	4.74	Plateau near (0.75, 0.25, 0.25)	...	
5.36	5.31	Δ_{5}^{v}-Δ_{5}^{c} (0.7, 0.0, 0.0)	M_1	5.24
5.45	5.5	Δ_{5}^{v}-Δ_{5}^{c}	M_1	5.34
6.49	6.5	$L_{4,5}^{v}$-L_{6}^{c} (0.5, 0.5, 0.5)	M_1	6.42
6.92	6.8 [a]	L_{6}^{v}-$L_{4,5}^{c}$ (0.5, 0.5, 0.5)	M_1	6.81

[a] See Ref. 44.

TABLE XV. Theoretical and experimental reflectivity structure for InSb and their identifications, including the location in the Brillouin zone, energy, and symmetry of the calculated critical points.

InSb Reflectivity structure (eV)		Associated critical points, location in		Critical-point energy
Theory	Experiment [a]	zone	Symmetry	(eV)
1.99	1.98	$L_{4,5}^{v}$-L_{6}^{c} (0.5, 0.5, 0.5)	M_1	1.99
2.47	2.48	L_{6}^{v}-L_{6}^{c}	M_1	2.47
3.53	3.39	Γ_{8}^{v}- Γ_{7}^{c} (0.0, 0.0, 0.0)	M_0	3.16
3.80	3.78	Γ_{8}^{v}- Γ_{8}^{c}	M_0	3.59
		Δ_{5}^{v}-Δ_{5}^{c} (0.3, 0.0, 0.0)	M_1 M_0	3.3 3.7
4.18	4.23	Plateau near (0.7, 0.2, 0.2)	...	
4.54	4.56	Δ_{5}^{v}-Δ_{5}^{c} (0.5, 0.0, 0.0)	M_1	4.44
4.74	4.75		M_1	4.69
5.44	5.33	L_{4}^{v}-L_{6}^{c} (0.5, 0.5, 0.5)	M_1	5.26
6.16	5.96	L_{6}^{v}-$L_{4,5}^{c}$ (0.5, 0.5, 0.5)	M_1	5.97

[a] See Ref. 33.

TABLE XVI. Calculated valence-band electronic densities of states features compared to experiment for Ga zinc blendes.

	Compound					
	GaP		GaAs		GaSb	
Feature	Theory	Experiment	Theory	Experiment	Theory	Experiment
Γ_1	−13.0	−11.8±0.5[a] −13.2±0.4[b]	−12.1	−12.9±0.5[a] −13.8±0.4[b]	−12.0	−11.6±0.3[b]
X_1	− 9.5	− 9.7±0.3[a] − 9.6±0.3[b]	− 9.9	−10.0±0.2[a] −10.7±0.2[b]	− 9.3	− 9.4±0.2[b]
X_3	− 7.1	− 6.9±0.2[a] − 6.9±0.3[b]	− 6.9	− 6.9±0.2[a] − 7.1±0.2[b]	− 6.8	− 6.9±0.3[b]
$\Sigma_1^{\min}$	− 4.2	− 4.1±0.2[a] − 4.0±0.3[b]	− 4.2	− 4.1±0.2[a] − 4.4±0.2[b]	− 3.6	− 3.8±0.2[b]
X_5	− 2.7	− 2.7±0.2[b]	− 2.9	•••	− 2.5	− 2.7±0.2[b]
L_3	− 1.1	− 0.8±0.2[a] − 1.2±0.3[b]	− 1.3	− 0.8±0.2[a] − 1.4±0.3[b]	− 1.2	− 1.3±0.2[b]

[a] See Refs. 3 and 6.
[b] See Refs. 2 and 5.

ably lower in magnitude than experiment. At higher energies, above the E_2, the situation is reversed, and the theoretical reflectivity is higher in magnitude than experiment. At present, the situation has not been clearly resolved, although considerable theoretical effort in this area has been undertaken.[47]

The electronic densities of states are displayed in Figs. 13 and 14 for the Ga and In compounds, respectively. In Tables XVI and XVII identifications of the structure are given and compared to the experimental results of photoemission spectroscopy. Our results do not include transition-matrix elements, therefore, only peak positions should be compared. In general, the XPS and UPS measurements are in good accord with respect to peak positioning. A possible exception to this is the placement of the lowest valence band. Differences in XPS and UPS for this band can be attributed, for the most part, to the methods used in data reduction.[5] In both techniques a rather large secondary background must be subtracted out to obtain the lowest band's position.

The overall agreement between the nonlocal results and experiment are a considerable improvement over the local pseudopotential results.[1] Local pseudopotential calculations are in disagreement with experimental data in some cases by the order of several electron volts.[4] The local results yield in the majority of cases, valence-band widths which are too narrow.

Two qualitative trends in the densities of states can be ascertained from an overview of the Ga and In compounds. As the lattice constant increases the valence band width decreases and as the crystal becomes more ionic, the gap occurring in the valence band increases. This latter trend has been related to changes in the antisymmetric part of the pseudopotential, and "ionicity."[48] While this approach has been somewhat successful, our charge density calculations indicate a more complicated situation.

In Figs. 15 and 16 the valence-charge densities are given for Ga and In compounds, respectively. These pseudocharge densities have received new interest not only because of recent experimental advances in x-ray techniques, but also because recent surface calculations have relied upon the pseudopotential charge density to determine a self-consistent pseudopotential.[52] In the case of InSb structure factors for quasiforbidden reflections have been experimentally determined.[10] These factors are a sensitive test of the asphericity of the valence charge density. A comparison of the experimental structure factors to the results as calculated by a local pseudopotential[22] indicates the local results overestimates the charge transfer from In to Sb. This comparison is complimented by an examination of the electronic density of states for the local pseudopotential. Such an examination indicates the calculated valence band widths are considerably narrower than the photoemission measurements would suggest. In turn this would also indicate an overestimation of the ionicity of the crystal. Therefore, it is not surprising that the nonlocal pseudopotential results for InSb, which yield an accurate valence band density of states, also yield an ac-

curate valence charge density.[53] The decrease in charge transfer for InSb with the nonlocal result is also reflected in the other compounds. In Tables XVIII and XIX the Fourier coefficients for the valence charge densities are given.

C. II-VI zinc-blende semiconductors

ZnSe and CdTe results are presented in this subsection. Local pseudopotential calculations have been fairly successful in describing optical reflectivities for II-VI's, but produce valence-band spectra in strong disagreement with experimental photoemission results. A recent local pseudopotential for CdTe, fit solely to reflectivity data, produced a valence-band width for the upper three valence bands in error by over 2 eV compared to experimental photoemission results.[54]

One difficulty in obtaining an accurate pseudopotential for these compounds is the proximity of the cation outermost d shell to the valence-band structure. In the case of ZnSe these states lie approximately 10 eV below the valence-band maximum.[5] Since the nonlocal pseudopotential used in the present calculation does not explicitly include these states, any effects of these states may not be accurately accounted for. Nevertheless, in the case of ZnSe, we are able to sig-

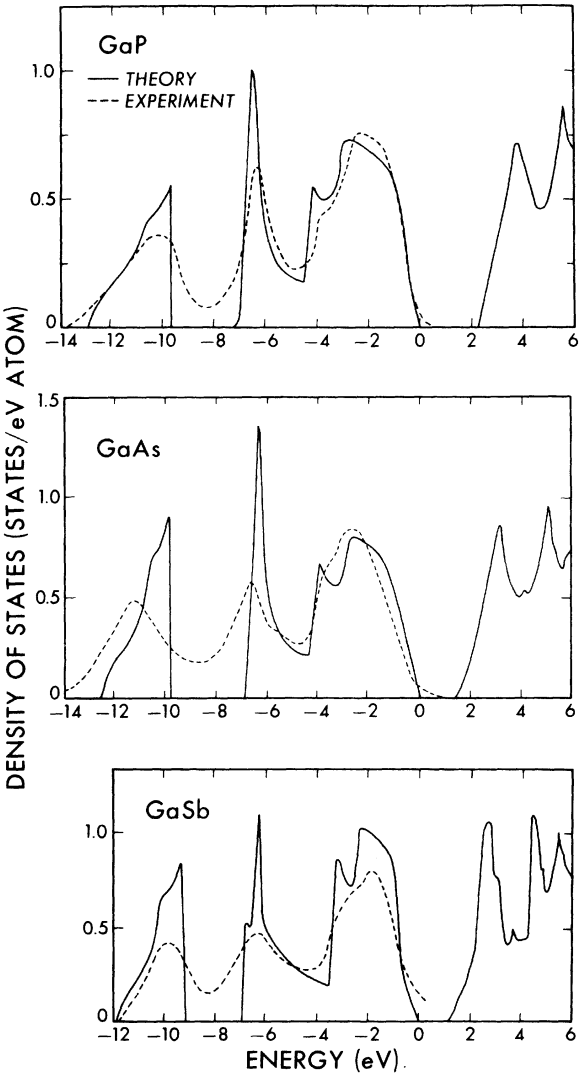

FIG. 13. Calculated electronic density of states, for GaP, GaAs, and GaSb compared to the experimental results of Ref. 5.

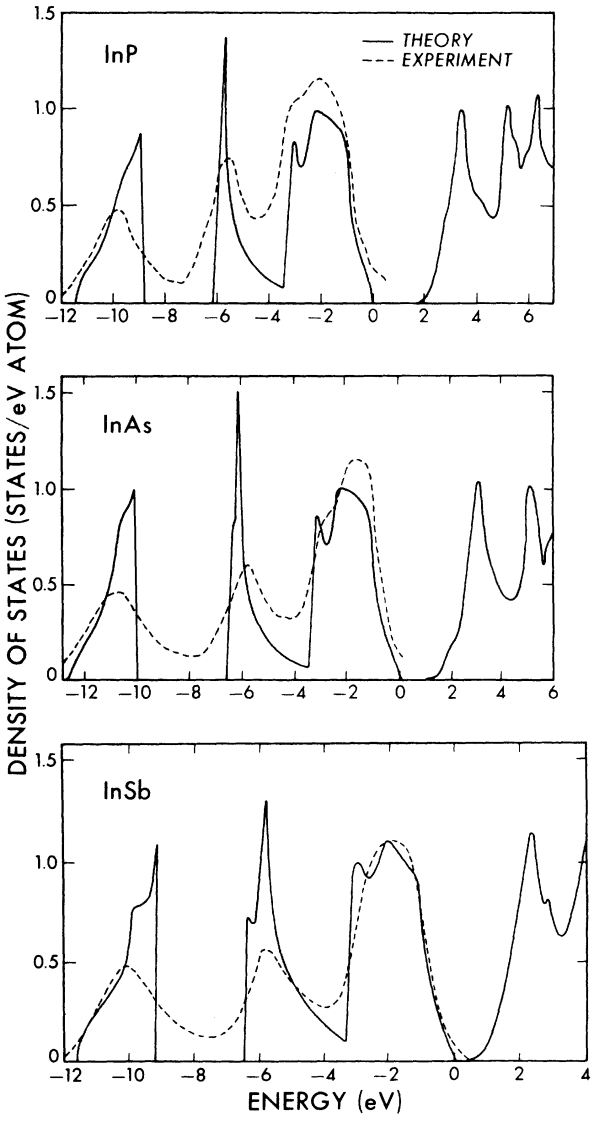

FIG. 14. Calculated electronic density of states for InP, InAs, and InSb compared to the experimental results of Ref. 5.

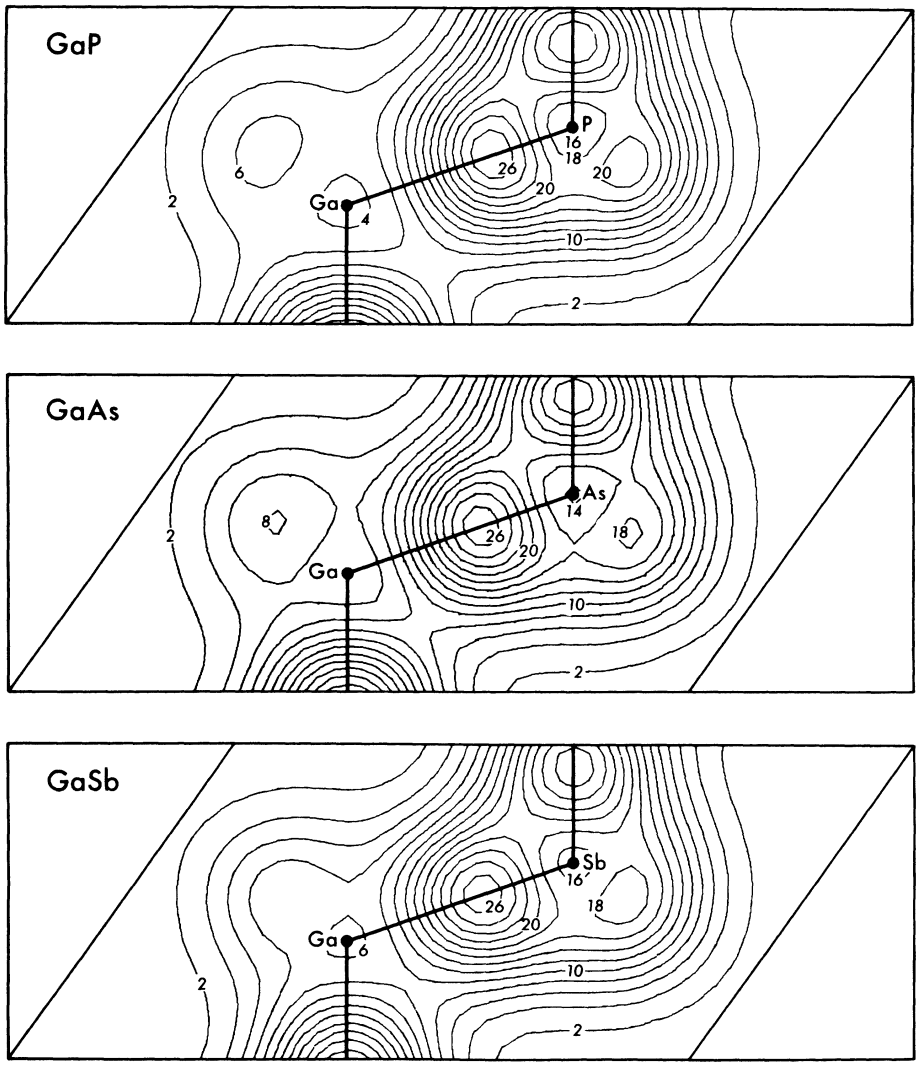

FIG. 15. Valence charge densities for GaP, GaAs, and GaSb. The contours are in units of (e/Ω_c).

nificantly improve the electronic density of states for the top three valence bands, and obtain reflectivity spectra giving satisfactory agreement between experiment and theory.[55] In the case of CdTe agreement is quite good for both the density of states and the optical spectra.

The parameters for the pseudopotential are listed in Table XX. Spin-orbit interactions are included in both cases: the spin-orbit parameters are 0.00061 and 0.00137 for ZnSe and CdTe, respectively. The band structures are given in Fig. 17 and the eigenvalues for Γ, X, and L in Table XXI. As expected, with the increased charge transfer in the II-VI's compared to the III-V's, the bandwidths decrease, and the optical gaps increase.

In Fig. 18 we present the calculated and experimental reflectivity spectra. Wavelength modulation experimental results are not available for these crystals. The overall agreement for ZnSe is satisfactory, but not as accurate as our III-V results; however, the result for CdTe is in good accord with experiment. One discrepancy occurring for both crystals, besides the magnitude of the reflectivity peaks, is the lack of agreement for the E_2 line shape. Experimentally, weak doublet structure is evident in the reflectivity spectra, but not observed in the theoretically calculated spectra. For both ZnSe and CdTe a band by band calculated absorption spectra indicate a weak M_1 critical point below the strong E_2 peak along the Δ direction. This structure, however, is too weak in the theoretical case to produce any significant structure. However, excitonic effects in the crystal may enhance the structure in experiment. Excitonic effects could also play a role in enhancing the E_1 structure which is consid-

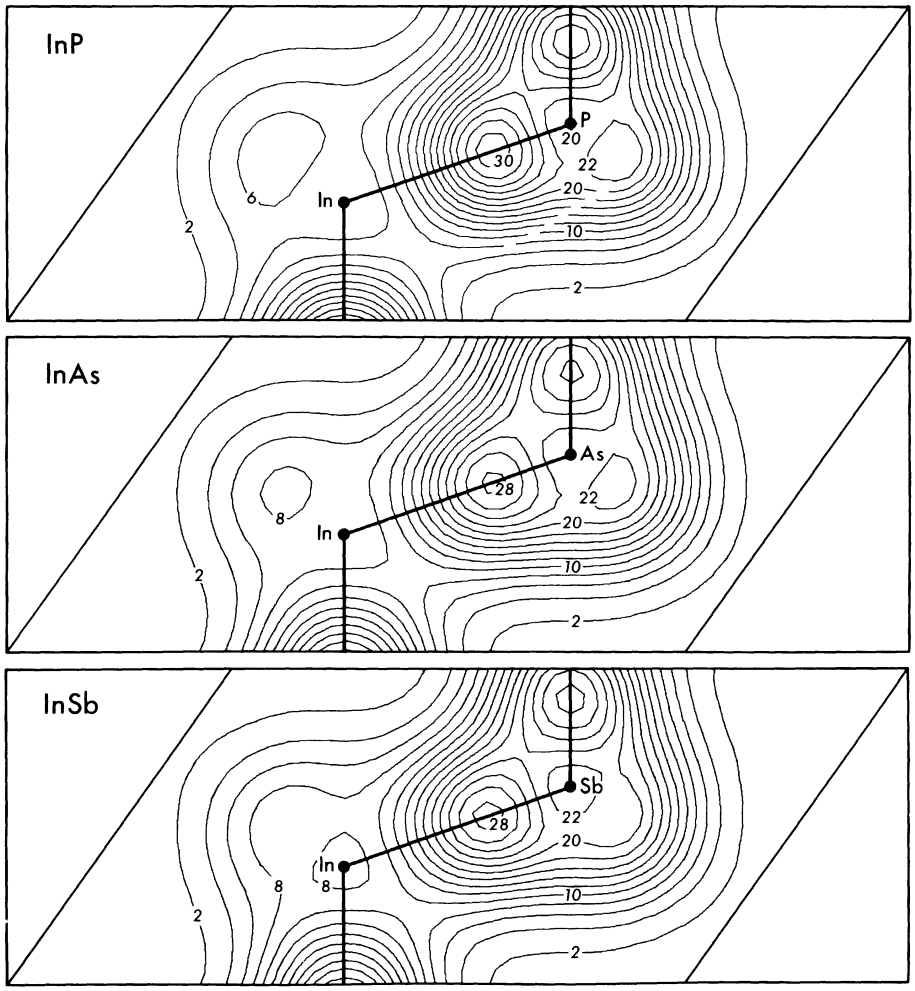

FIG. 16. Valence charge densities for InP, InAs, and InSb. The contours are in units of (e/Ω_c).

TABLE XVII. Calculated valence-band electronic densities of states features compared to experiment for In zinc blendes.

	Compound					
	InP		InAs		InSb	
Feature	Theory	Experiment	Theory	Experiment	Theory	Experiment
Γ_1	−11.4	−11.0 ± 0.4 [a]	−12.7	−12.3 ± 0.4 [a]	−11.7	−11.7 ± 0.3 [a] −11.2 ± 0.2 [b]
X_1	− 8.9	− 8.9 ± 0.3 [a]	−10.2	− 9.8 ± 0.3 [a]	− 9.2	− 9.5 ± 0.2 [a] − 9.0 ± 0.3 [b]
X_3	− 6.0	− 5.9 ± 0.2 [a]	− 6.2	− 6.3 ± 0.2 [a]	− 6.4	− 6.4 ± 0.2 [a] − 6.5 ± 0.3 [b]
$\Sigma_1^{\min}$	− 3.3	− 3.2 ± 0.2 [a]	− 3.4	− 3.3 ± 0.2 [a]	− 3.4	− 3.4 ± 0.2 [a] − 3.65 ± 0.3 [b]
X_5	− 2.1	− 2.0 ± 0.2 [a]	− 2.4	− 2.4 ± 0.3 [a]	− 2.3	− 2.4 ± 0.4 [a]
L_3	− 1.0	− 1.0 ± 0.3 [a]	− 1.1	− 0.9 ± 0.3 [a]	− 1.2	− 1.4 ± 0.3 [a] − 1.05 ± 0.3 [b]

[a] See Refs. 2 and 5.
[b] See Refs. 3 and 6.

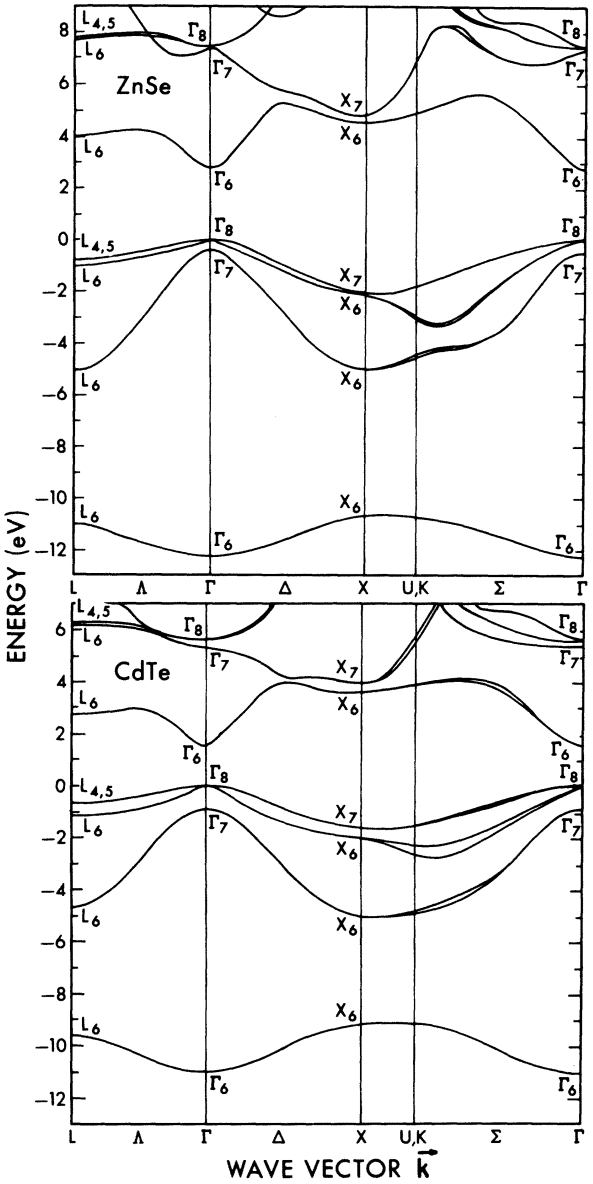

FIG. 17. Band structures for ZnSe and CdTe.

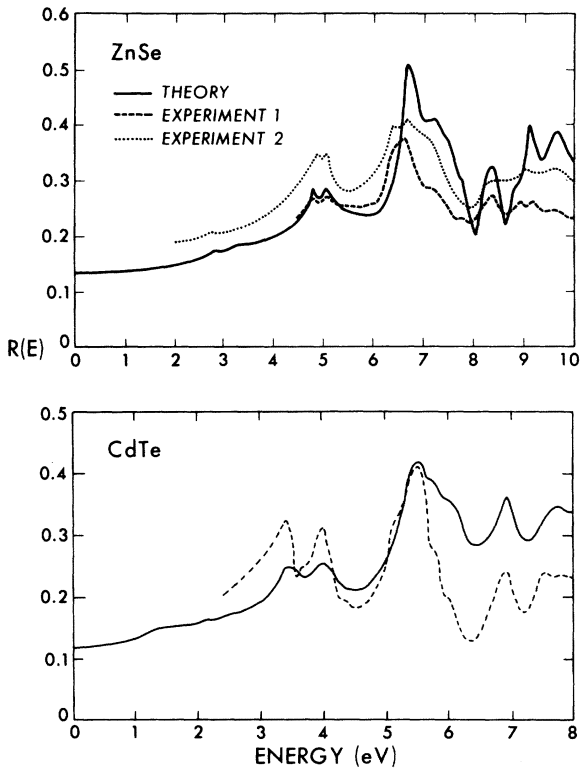

FIG. 18. Calculated reflectivity spectra for ZnSe and CdTe compared to experiment. The experimental results for ZnSe are from Ref. 49 (dashed line) and from Ref. 50 (dotted line). For CdTe the experimental results are from Ref. 51.

TABLE XVIII. Fourier coefficients of the valence charge densities for the Ga zinc blendes. The real part of the coefficient is listed first. The origin for this calculation is at the cation.

$\vec{G}(a/2\pi)$	Fourier coefficients (e/Ω_c) GaP		GaAs		GaSb	
(000)	8.000	0.000	8.000	0.000	8.000	0.000
(111)	0.648	−1.880	0.826	−1.755	1.000	−1.792
(200)	−0.924	0.000	−0.656	0.000	−0.577	0.000
(220)	−0.049	0.000	−0.082	0.000	0.047	0.000
(311)	−0.219	−0.198	−0.256	−0.269	−0.210	−0.215
(222)	0.095	−0.355	0.059	−0.452	0.044	−0.421
(400)	−0.191	0.000	−0.259	0.000	−0.235	0.000
(331)	0.056	0.070	0.053	0.026	0.038	0.027
(420)	0.070	0.000	0.050	0.000	0.045	0.000
(422)	−0.037	0.032	−0.024	0.020	−0.033	0.013

TABLE XIX. Fourier coefficients of the valence charge densities for the In zinc blendes. The real part of the coefficient is listed first. The origin for this calculation is at the cation site.

$\vec{G}(a/2\pi)$	Fourier coefficients (e/Ω_c) InP		InAs		InSb	
(000)	8.000	0.000	8.000	0.000	8.000	0.000
(111)	0.801	−2.067	0.885	−1.998	0.994	−1.915
(200)	−1.013	0.000	−0.860	0.000	−0.718	0.000
(220)	0.097	0.000	0.135	0.000	0.144	0.000
(311)	−0.255	−0.160	−0.200	−0.151	−0.223	−0.161
(222)	0.048	−0.439	0.030	−0.437	0.020	−0.409
(400)	−0.237	0.000	−0.215	0.000	−0.245	0.000
(331)	0.071	0.063	0.040	0.047	0.045	0.038
(420)	0.069	0.000	0.055	0.000	0.048	0.000
(422)	−0.046	0.043	−0.042	0.020	−0.043	0.024

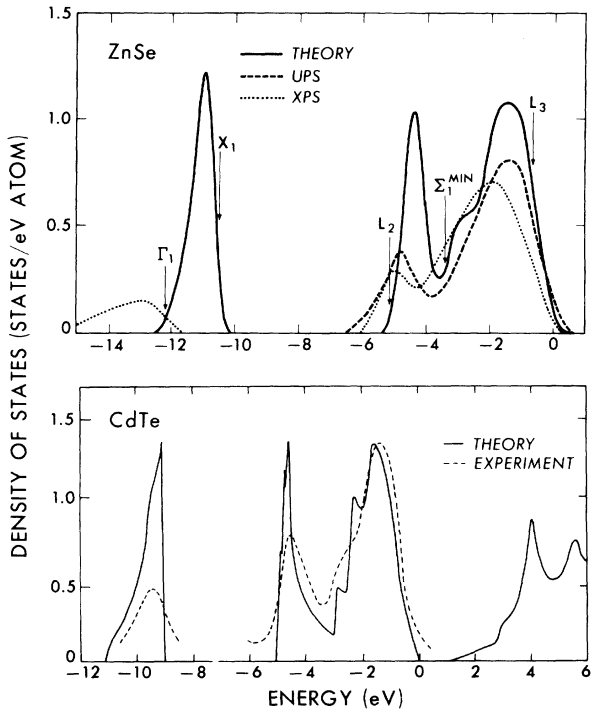

FIG. 19. Calculated valence-band electronic densities of states for ZnSe and CdTe compared to experiment. The experimental results for ZnSe are from Ref. 5 (dotted line) and Ref. 6 (dashed line). For CdTe the experimental results are from Ref. 6.

erably stronger in experiment than the theoretical result for either ZnSe or CdTe. The prominent reflectivity structures for both ZnSe and CdTe are identified and compared with experiment in Tables XXII and XXIII, respectively.

In Fig. 19 the theoretical electronic density of states are compared to the experimental results of photoemission. The outermost d-shell contributions have been subtracted out of the experimental spectra. Identifications and comparisons of the experimental structure with the theoretical results are listed in Table XXIV. While CdTe is in good agreement with experiment, ZnSe is not as satisfactory; the bottom valence band is in strong discrepancy with the XPS placement. Unfortunately, the lowest valence band is not observed in the UPS results. However, recent reflectivity data have suggested a higher placement for this bottom valence band. Using synchrotron radiation, studies have been made of II-VI reflectivity spectra. Structure for ZnSe has been observed in the 15–16-eV range and attributed to the onset of optical transitions from the lowest valence band.[50] If we accept this identification, the reflectivity result would be in accord with the nonlocal pseudopotential placement.

The valence charge densities for ZnSe and CdTe are displayed in Fig. 20; the Fourier coefficients of the charge densities are listed in Table XXV. Our results are in contrast to the local pseudopotential charge densities[22]; these

TABLE XX. Pseudopotential parameters for the II-VI zinc-blende semiconductors.

Compound	$V^S(\sqrt{3})$	$V^S(\sqrt{8})$	$V^S(\sqrt{11})$	$V^A(\sqrt{3})$	$V^A(\sqrt{4})$	$V^A(\sqrt{11})$	Lattice constant (Å)
ZnSe	−0.218	0.029	0.064	0.139	0.062	0.016	5.65
CdTe	−0.220	0.00	0.062	0.060	0.050	0.025	6.48

	Nonlocal parameters					
	Cation			Anion		
Compound	β_0	A_2(Ry)	R_0(Å)	β_0	A_2(Ry)	A_0(Å)
ZnSe [a]	0	−0.125	0	0	0.925	0
CdTe	0.4	0.00	1.37	0.4	2.00	1.06

[a] Gaussian well.

results would suggest a nearly complete charge transfer from cation to anion. The nonlocal pseudopotential results indicate a strong, but not complete, charge transfer. This result can be attributed directly to the effect of the nonlocal d well. The d-well correction term alters the conduction bands without affecting the occupied valence states. Thus it is possible for the d well to alter the optical gaps and not alter the charge density. The local pseudopotential yields optical gaps which are too narrow, in general, as compared to experiment. If an accurate fit is attempted to these gaps, the antisymmetric form factors must be increased. This procedure has two defects: the valence-band widths decrease, a trend not supported by XPS or UPS data and the charge transfer increases, the crystal becomes unphysically ionic.

IV. CONCLUSION

Nonlocal pseudopotentials have been used to calculate the electronic structure of 11 semiconductors. Detailed comparisons have been presented for the theoretical reflectivity spectra and valence-band electronic densities of states and the experimental reflectivity and photoemission results. In the case of Si and InSb recent

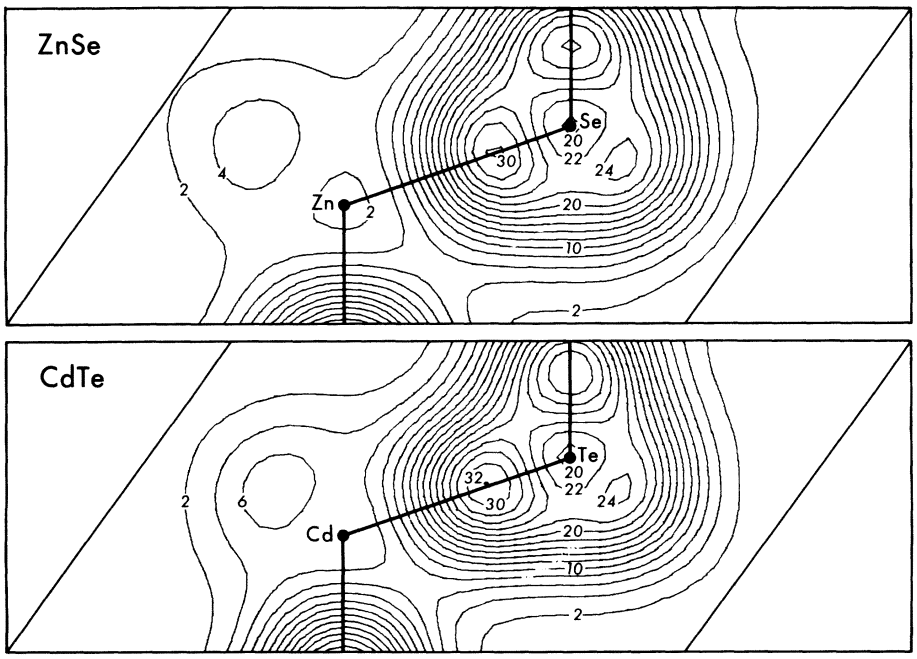

FIG. 20. Valence charge densities for ZnSe and CdTe. The contours are in units (e/Ω_c).

TABLE XXI. Eigenvalues for the II-VI zinc-blende semiconductors at Γ, X, and L. Energies are in eV.

Point	Level	Compound ZnSe	Compound CdTe
Γ	Γ_6^v	−12.25	−11.07
	Γ_7^v	− 0.45	− 0.89
	Γ_8^v	0.00	0.00
	Γ_6^c	2.76	1.59
	Γ_7^c	7.33	5.36
	Γ_8^c	7.42	5.61
X	X_6^v	−10.72	− 9.12
	X_6^v	− 4.96	− 5.05
	X_6^v	− 2.17	− 1.98
	X_7^v	− 1.96	− 1.60
	X_6^c	4.54	3.48
	X_7^c	5.17	3.95
L	L_6^v	−11.08	− 9.64
	L_6^v	− 5.08	− 4.73
	L_6^v	− 1.04	− 1.18
	$L_{4,5}^v$	− 0.76	− 0.65
	L_6^c	3.96	2.82
	L_6^c	7.68	6.18
	$L_{4,5}^c$	7.72	6.35

experimental results using x rays have allowed us to assess the pseudocharge densities. We find that numerous discrepancies which occur for local pseudopotential calculations can be removed. The discrepancies in the case of a local pseudopotential include obtaining incorrect valence-band widths, optical critical point symmetries, optical band gaps, bonding charge topologies, and valence-charge transfers.

While the nonlocal pseudopotential results do not suffer from these defects, the method does require additional parameters. This requirement does not present any special problems provided experimental data such as photoemission are included in the parameter fitting. Further, various trends in the nonlocal pseudopotential parameters can be observed and correlated with model pseudopotential calculations. For example, in the Ge and α-Sn row we find the d-well correction increases from Zn to Se and from Cd to Te. This trend is also observed in the Heine-Abavenkov model pseudopotential.[17] Thus, while our approach has been decidedly empirical in nature, the great success of our nonlocal results suggests other, less empirical, methods may be refined to give equally accurate results.

Part of this work was done under the auspices of the U. S. Energy Research and Development Administration.

TABLE XXII. Theoretical and experimental reflectivity structure at 300 °K and their identifications, including the location in the Brillouin zone, energy, and symmetry of the calculated critical points for ZnSe. The experimental results are from Ref. 49.

ZnSe reflectivity structure (eV) Theory	Experiment	Associated transitions located in the zone	Symmetry	Critical-point energy (eV)
4.79	4.75	$L_{4,5}^v - L_6^c$ (0.5, 0.5, 0.5)	M_1	4.72
5.06	5.05	$L_6^v - L_6^c$	M_1	5.00
...	6.00	...	...	...
(6.6) [a]	6.50	$\Delta_5^v - \Delta_5^c$ (0.5, 0.0, 0.0)	M_0	6.55
6.71	6.63	Plateau near (0.8, 0.2, 0.2)	...	
7.22	7.15	$\Delta_5^v - \Delta_5^c$ (0.6, 0.0, 0.0)	M_1	7.08
7.47	7.60	$\Gamma_8^v - \Gamma_8^c$ (0.0, 0.0, 0.0)	M_0	7.42
7.76	7.80	$\Gamma_7^v - \Gamma_8^c$	M_0	7.87
8.39	8.45	$L_{4,5}^v - L_{4,5}^c, L_6^c$ (0.5, 0.5, 0.5)	M_0	8.46
		$\Lambda_{4,5} - \Lambda_{4,5}, \Lambda_6^c$ (0.35, 0.35, 0.35)	M_1	8.48
8.86	8.97	$L_6^v - L_{4,5}, L_6^c$ (0.5, 0.5, 0.5)	M_0	8.74
		$\Lambda_6^v - \Lambda_{4,5}, \Lambda_6^c$ (0.35, 0.35, 0.35)	M_1	8.76

[a] See text.

TABLE XXIII. Theoretical and experimental reflectivity structure for CdTe and their identifications, including the location in the Brillouin zone, energy, and symmetry of the calculated critical points. The experiment is from Ref. 51.

CdTe Reflectivity structure (eV)		Associated critical points location in		Critical-point energy
Theory	Experiment	zone	Symmetry	(eV)
1.65	1.59	$\Gamma_8^v - \Gamma_7^c$ (0.0, 0.0, 0.0)	M_0	1.59
3.49	3.46	$L_{4,5}^v - L_6^c$ (0.5, 0.5, 0.5)	M_1	3.47
4.04	4.03	$L_6^v - L_6^c$	M_1	4.00
5.16	5.18	$\Delta_5^v - \Delta_5^c$ (0.5, 0.0, 0.0)	M_0	5.14
5.50	5.53	Plateau near (0.75, 0.25, 0.25)	...	
5.68	5.68	$\Delta_5^v - \Delta_5^c$ (0.75, 0.0, 0.0)	M_1	5.58
6.00	5.95	$\Delta_5^v - \Delta_5^c$	M_1	5.96
6.91	6.82	$L_{4,5}^v - L_6^c$ (0.5, 0.5, 0.5)	M_1	6.83
...	7.44			
7.79	7.6	$L_6^v - L_{4,5}^c$ (0.5, 0.5, 0.5)	M_1	7.53

TABLE XXIV. Calculated valence-band electronic densities of states features compared to experiment for II-VI zinc blendes.

	Compound			
	ZnSe		CdTe	
Feature	Theory	Experiment	Theory	Experiment
Γ_1	−12.3	-15.2 ± 0.6 [a]	−11.1	...
X_1	−10.7	-12.5 ± 0.4 [a]	− 9.1	-8.8 ± 0.3 [b]
X_3	− 5.1	-5.6 ± 0.3 [a] -5.3 ± 0.3 [b]	− 5.2	-5.1 ± 0.2 [a] -4.7 ± 0.2 [b]
$\Sigma_1^{\min}$	− 3.4	-3.4 ± 0.2 [a] -3.4 ± 0.3 [b]	− 2.7	-2.7 ± 0.3 [a] -2.8 ± 0.2 [b]
X_5	− 2.2	-2.1 ± 0.3 [a]	− 1.7	-1.8 ± 0.2 [a]
L_3	− 1.0	-1.3 ± 0.3 [a] -0.7 ± 0.2 [b]	− 0.9	-0.9 ± 0.3 [a] -0.7 ± 0.2 [b]

[a] See Refs. 2 and 5.
[b] See Refs. 3 and 6.

TABLE XXV. Fourier coefficients of the valence charge densities for the II-VI zinc-blende semiconductors. The real part of the coefficient is tabulated first. The origin is at the cation site.

	Fourier coefficients (e/Ω_c)			
$\vec{G}(a/2\pi)$	ZnSe		CdTe	
(000)	8.000	0.000	8.000	0.000
(111)	0.428	−2.233	0.851	−2.210
(200)	−1.235	0.000	−1.063	0.000
(220)	0.004	0.000	0.130	0.000
(311)	−0.210	−0.216	−0.257	−0.199
(222)	0.085	−0.363	0.052	−0.470
(400)	−0.225	0.000	−0.296	0.000
(331)	0.069	0.081	0.058	0.060
(420)	0.096	0.000	0.080	0.000
(422)	−0.040	0.038	−0.054	0.022

*Supported by the NSF under the Grant No. DMR72-03206-A02.
†NSF Postdoctoral Fellowship.
‡Present address: Bell Laboratories, Murray Hill, N. J. 07974.

[1]M. L. Cohen and V. Heine, Solid State Phys. 24, 37 (1970).
[2]R. Pollak, L. Ley, S. Kowalcyzk, D. A. Shirley, J. Joannopoulos, D. J. Chadi, and M. L. Cohen, Phys. Rev. Lett. 29, 1103 (1973).
[3]W. D. Grobman and D. E. Eastman, Phys. Rev. Lett. 29, 1508 (1972).
[4]J. R. Chelikowsky, D. J. Chadi, and M. L. Cohen, Phys. Rev. B 8, 2786 (1973).
[5]L. Ley, R. A. Pollak, F. R. McFeely, S. P. Kowalcyzk, and D. A. Shirley, Phys. Rev. B 9, 600 (1974).

[6]D. E. Eastman, W. D. Grobman, J. L. Freeouf, and M. Erbudak, Phys. Rev. B 9, 3473 (1974).
[7]J. R. Chelikowsky and M. L. Cohen, Phys. Rev. Lett. 31, 1582 (1973).
[8]K. C. Pandey and J. C. Phillips, Phys. Rev. B 9, 1552 (1974).
[9]Y. W. Yang and P. Coppens, Solid State Commun. 15, 1555 (1974).
[10]D. H. Bilderback and R. Colella, Phys. Rev. Lett. 35, 858 (1975).
[11]J. C. Phillips and L. Kleinman, Phys. Rev. 116, 287 (1959).
[12]J. C. Phillips and K. C. Pandey, Phys. Rev. Lett. 30, 787 (1973).
[13]J. R. Chelikowsky and M. L. Cohen, Phys. Rev. Lett. 32, 674 (1974).
[14]M. L. Cohen and T. K. Bergstresser, Phys. Rev. 141, 789 (1966), and those listed in Ref. 1.
[15]J. R. Chelikowsky and M. L. Cohen, Phys. Rev. B 10, 5025 (1974).
[16]D. Brust, Phys. Rev. B 4, 3497 (1971).
[17]I. V. Abrenkov and V. Heine, Philos. Mag. 12, 529 (1965); and A. O. E. Animalu and V. Heine, *ibid.* 12, 1249 (1965).
[18]C. D. Chekroun, I. B. Ortenberger, and F. Herman, Bull. Am. Phys. Soc. 18, 322 (1973).
[19]G. Gilat and L. J. Raubenheimer, Phys. Rev. 144, 390 (1966).
[20]D. J. Chadi and M. L. Cohen, Phys. Rev. B 8, 5747 (1973).
[21]A. Baldereschi, Phys. Rev. B 7, 5212 (1973).
[22]J. P. Walter and M. L. Cohen, Phys. Rev. B 4, 1877 (1971).
[23]D. J. Chadi (private communication).
[24]L. R. Saravia and D. Brust, Phys. Rev. 176, 915 (1968).
[25]G. Weisz, Phys. Rev. 149, 504 (1966).
[26]S. Bloom and T. K. Bergstresser, Solid State Commun. 6, 465 (1970).
[27]J. P. Walter, M. L. Cohen, Y. Petroff, and M. Balkanski, Phys. Rev. B 1, 2661 (1970).
[28]F. Herman and S. Skillman, *Atomic Structure Calculations* (Prentice-Hall, Englewood Cliffs, N. J., 1963).
[29]Rather than employing a square-well correction term a Gaussian nonlocal correction term was used for Ge, GaAs, and ZnSe. See Refs. 7, 13, and 55.
[30]H. R. Philipp and H. Ehrenreich, Phys. Rev. 129, 1550 (1963).
[31]M. Cardona, P. McElroy, F. H. Pollak, and K. L. Shaklee, Solid State Commun. 4, 319 (1966); and P. T. McElroy, Technical Report No. HP-21 (ARPA-54), Division of Engineering and Applied Physics, Harvard University (unpublished).
[32]R. R. L. Zucca, J. P. Walter, Y. R. Shen, and M. L. Cohen, Solid State Commun. 8, 627 (1970).
[33]R. R. L. Zucca and Y. R. Shen, Phys. Rev. B 1, 2668 (1970).
[34]M. Welkowsky and R. Braunstein, Phys. Rev. B 5, 497 (1972).
[35]F. H. Pollak, M. Cardona, C. W. Higginbotham, F. Herman, and J. P. Van Dyke, Phys. Rev. B 2, 352 (1970).
[36]D. E. Aspnes, Phys. Rev. Lett. 31, 230 (1973).
[37]See Refs. 31 and 35.
[38]W. E. Spicer and R. C. Eden, *Proceedings of the Ninth International Conference of the Physics of Semiconductors, Moscow, 1968* (Nauka, Leningrad, 1969) Vol. 1, p. 61.
[39]J. C. Phillips, Rev. Mod. Phys. 42, 317 (1970).
[40]S. S. Vishnubhatla and J. C. Woolley, Can. J. Phys. 46, 1769 (1968).
[41]M. Cardona, J. Appl. Phys. Suppl. 32, 2151 (1961).
[42]C. Varea de Alvarez, J. P. Walter, M. L. Cohen, J. Stokes, and Y. R. Shen, Phys. Rev. B 6, 1412 (1972).
[43]M. Cardona, in *Semiconductors and Semimetals*, edited by R. Willardson and A. Beer (Academic, New York, 1967), Vol. 3, p. 138.
[44]H. Ehrenreich, H. R. Philipp, and J. C. Phillips Phys. Rev. Lett. 8, 59 (1962).
[45]A. M. Gray, Phys. Status Solidi 37, 11 (1970).
[46]D. E. Aspnes and A. A. Studna, Phys. Rev. B 7, 4605 (1973).
[47]See, for example, J. A. Van Vechten and R. M. Martin, Phys. Rev. Lett. 28, 446 (1972); W. R. Hanke and L. J. Sham, *ibid.* 33, 582 (1974); and S. G. Louie, J. R. Chelikowsky, and M. L. Cohen, *ibid.* 34, 155 (1975).
[48]D. J. Chadi, M. L. Cohen, and W. D. Grobman, Phys. Rev. B 8, 5587 (1973).
[49]J. P. Walter, M. L. Cohen, Y. Petroff, and M. Balkanski, Phys. Rev. B 1, 2661 (1970).
[50]J. L. Freeouf, Phys. Rev. B 7, 3810 (1973).
[51]D. J. Chadi, J. P. Walter, M. L. Cohen, Y. Petroff and M. Balkanski, Phys. Rev. B 5, 3058 (1972).
[52]J. A. Appelbaum and D. R. Hamann, Phys. Rev. B 8, 1777 (1973); and Phys. Rev. Lett. 32, 225 (1974).
[53]J. R. Chelikowsky and M. L. Cohen, Phys. Rev. Lett. 36, 229 (1976).
[54]D. J. Chadi, J. P. Walter, M. L. Cohen, Y. Petroff, and M. Balkanski, Phys. Rev. B 5, 3058 (1972).
[55]J. R. Chelikowsky and M. L. Cohen, Phys. Lett. A 47, 7 (1974).